SNOWFLAKE SHAPED HIGH CONDUCTIVITY INSERTS FOR HEAT TRANSFER ENHANCEMENT

A Thesis submitted to
the Graduate School of Engineering and Sciences of
İzmir Institute of Technology
in Partial Fulfillment of the Requirements for the Degree of

MASTER OF SCIENCE

in Mechanical Engineering

by
Hasel Çiçek KONAN

July 2018
İZMİR

We approve the thesis of **Hasel Çiçek KONAN**

Examining Committee Members:

Assoc. Prof. Dr. Erdal ÇETKİN
Department of Mechanical Engineering, İzmir Institute of Technology

Prof. Dr. Aytunç EREK
Department of Mechanical Engineering, Dokuz Eylül University

Assist. Prof. Dr. Murat BARIŞIK
Department of Mechanical Engineering, İzmir Institute of Technology

9 July 2018

Assoc. Prof. Dr. Erdal ÇETKİN
Supervisor, Department of Mechanical Engineering,
İzmir Institute of Technology

Prof. Dr. Metin TANOĞLU
Head of the Department of
Mechanical Engineering

Prof. Dr. Aysun SOFUOĞLU
Dean of the Graduate School of
Engineering and Sciences

ACKNOWLEDGMENTS

Firstly, I would like to thank my advisor Erdal ÇETKİN for his guidance, help and patience during the thesis. In addition, I would like to thank Prof. Dr. Aytunç EREK and Assist. Prof. Dr. Murat BARIŞIK to have time for my thesis defense exam. I also would like to my friend Elias OUEDRAOGO for beneficial discussions about heat transfer.

Lastly, I would like to thank my family, Elmas, Hasan and Süleyman Emre Konan for their endless support and patience.

ABSTRACT

SNOWFLAKE SHAPED HIGH CONDUCTIVITY INSERTS FOR HEAT TRANSFER ENHANCEMENT

In this study we show numerically how thermal resistance in a two-dimensional domain with a point heat source can be reduced with embedded high-conductivity snowflake shaped pathways. The external shape of the domain is square, and its boundaries are adiabatic. Rectangular fins were used as high-conductivity pathways in order to minimize maximum excess temperature (T_{max}). The geometry of the inserted pathways was optimized with consideration of Constructal Theory for minimum T_{max}. In the first assembly, optimum number of mother (big) fins was uncovered as the area fraction increases. The results of the first assembly indicate that the increase in the number of mother fins does not increase heat transfer after a limit number for the fins, i.e., optimum number of mother fins exits. After uncovering the mother pathway geometry corresponding to the minimum T_{max}, the daughter (small) fins inserted at the tip of them, i.e. second assembly. In the second assembly, the fin ratios, small fin location and angle between daughter fins were discovered when the area fraction is fixed. In addition, in the third assembly, larger daughter fins were attached to mother fins. The results of the second and third assemblies document what should be the geometric length scales and the number of daughter fins in order to minimize T_{max}. The optimized design uncovers that the fins should be designed similar to snowflake shape. Therefore, the results also uncover snowflakes correspond to the designs with minimum thermal conductivity, i.e., not mimicking the nature but understanding it with physics.

Keywords and Phrases: Heat transfer enhancement, Fins, Constructal Theory, Snowflake

ÖZET

ISI TRANSFER ARTTIRIMI İÇİN KARTANESİ ŞEKİLLİ YÜKSEK İLETİMLİ EKLENTİLER

Bu çalışmada noktasal bir ısı kaynağı içeren iki boyutlu yapıda ısıl direncin kar tanesi şeklindeki yüksek iletkenli eklentilerle nasıl azaltılabileceğini sayısal olarak gösteriyoruz. Yapının dış şekli bir kare ve karenin sınırları ısı geçirmezdir. Yüksek iletkenli eklentiler olarak dikdörtgen eklentiler kullanıldı. En düşük en yüksek sıcaklığı elde etmek için eklentilerin şekli yapısal gelişim teorisine göre geliştirildi. Birinci eklemede, alan oranı arttırılarak anne (büyük) eklentilerin optimal sayısı bulundu. İlk eklemdeki sonuçlara göre, anne eklentilerin sayısındaki artış belirli bir sayıdan sonra ısı iletimini arttırmıyor. Bu durum anne eklentiler için optimal bir sayının olduğunu gösteriyor. Optimal eklenti sayısı, düşük ısıl iletkenli bölgedeki ısıl direnci azaltmak için uygun kısa aralıkları ve bir yalıtım katmanı gibi davranan ısıl sınır katmanlarını ortadan kaldıran uygun uzun aralıkları tasarlamaya benzerdir. En düşük en yüksek sıcaklık için anne eklentilerin geometrisi açığa çıktıktan sonra, yavru (küçük) eklentiler anne eklentilerin ucuna eklendi. Yavru eklentilerin eklenmesi ikinci eklemeyi başlattı. İkinci eklemede alan oranı sabit olduğu zaman, yavru eklentilerin optimal boyut oranları, yavru eklentilerin yeri ve onların arasındaki optimal açı bulundu. Daha büyük yavru eklentiler de anne eklentilere üçüncü eklemede eklendi. İkinci ve üçüncü eklemenin sonuçları, en yüksek sıcaklığı azaltmak için yavru eklentilerin geometrik uzunluk ölçütünün ne olması gerektiğini ve onların sayıları gösteriyor. Optimal tasarım, eklentilerin kar tanesi şekline benzer şekilde tasarlanması gerektiğini ortaya çıkarıyor. Bu sonuçlar kar tanesinin en az ısıl dirence sahip tasarıma uygun olduğunu ortaya çıkarıyor. Bu sonuca doğayı kopyalayarak değil, fiziği anlayarak ulaştık.

Anahtar Kelimeler ve İfadeler: Isı İletimi Arttırılması, Yüksek İletkenli Eklentiler, Yapısal Gelişim Teorisi, Kar tanesi

TABLE OF CONTENTS

LIST OF FIGURES

LIST OF TABLES

Table **Page**

LIST OF SYMBOLS

A	Area	m^2
k	Thermal conductivity	$W/(mK)$
t_f	Thickness of mother fin	m
L_f	Length of mother fin	m
L	Length of square	m
m	Number of mother fins	
n	Vector normal to solid-solid interface	
T	Temperature	K
q''	Heat flux	W/m^2
x, y	Spatial coordinates	
#	The number of	

Greek Letters

ϕ	Volume fraction
α	Angle between small fins

Subscripts

b	Big
h	High
f	Fin
l	Low
max	Maximum
opt	Optimum
s	Small
sur	Surface

Superscripts

i	Index of mesh independency test

CHAPTER 1

INTRODUCTION

While the size of electronic equipment decreasing, the number of components and their process capability in those devices are being increased. Therefore, dissipation of heat from the systems while keeping the temperature under a limit temperature becomes more challenging [1]. Convection heat transfer mechanisms would not be suitable in miniaturized designs as they require additional space for working fluid, piping and additional equipment. Conduction heat transfer occurs molecular activity. Therefore, conductive heat transfer mechanism becomes more advantageous in miniaturized designs. Bejan [2] stated that conductive pathways are very influential to enhance heat transfer if they are optimized considering Constructal Theory.

Constructal Theory represents a new approach, which includes evolution of flow (heat or fluid) configuration depending on physical principles. Constructal Law was stated by Adrian Bejan as "For a finite-size flow system to persist in time (to live), its configuration must change in time such that it provides easier and easier access to its current." The Constructal Law statement emphasizes that a flow system should change its shape to minimize flow resistance in order to survive. Therefore, minimization of resistance to the flow can be deduced from the Constructal Theory statement even it is a lot broader in sense as Bejan stated in 1996. The configuration is a major unknown and it is observed in animate and inanimate systems. The Constructal Law is a guide to uncover the configurations of natural systems and to create new configurations for engineering systems [3]. Constructal Law is applicable in many distinct fields. For instance, Bejan et al. [4] showed that cost minimization is possible for point- to-area or area-to-point transportation. Reis et al. [5] analytically showed the number of bifurcations before alveolar trachea in the respiratory system corresponds to the minimum flow resistance. In addition, Bejan and Lorente [6] stated that fluid flows in river basins similar to tree-shaped structures. Furthermore, Azad and Amidpour [7] designed optimized shell and tube heat exchanger in order to decrease pumping and capital cost for the system.

1.1. High-conductivity Pathways

Bejan [2] stated that how high-conductivity paths should be designed from a surface to one point (heat sink) to minimize the thermal resistance while heat is generated in low conductivity domain volumetrically and uniformly. He analytically uncovered the design corresponding to the minimum thermal resistance for domain, shown in Figure 1. Firstly, Bejan optimized the external shape (H_1/L_1) and $(H_1/L_1)_{opt}$ is 2. Then, the design of the high-conductivity pathways was optimized. The optimization results show that when the number of assemblies is increased, the scale of constituents become smaller and thinner. In addition, Bejan indicated that the configuration of the paths should be tree-shaped to minimize T_{max}.

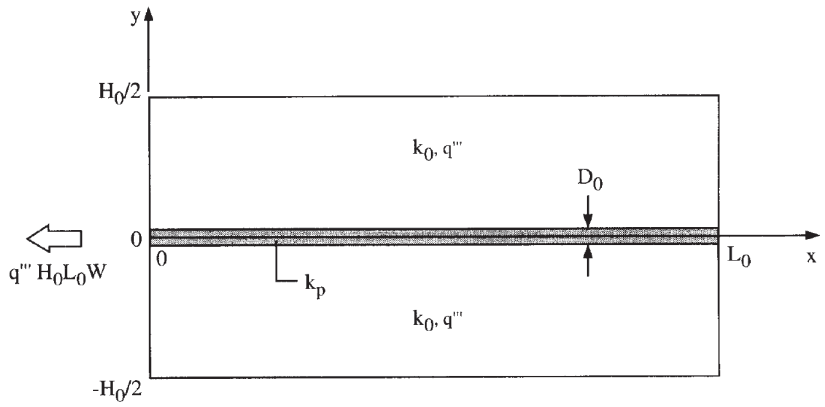

Figure 1. High-conductivity pathway in a heat generating volume [2]

Ledezma et al. [8] optimized numerically for all geometric properties in a heat generating domain as shown in Figure 2. They uncovered the shape of the largest assembly, constituents of assemblies and the number of branches. They stated that the configuration of high-conductivity pathways should have a tree shape. The number of branches and their thickness vary depends on complexity of the configuration.

Almogbel and Bejan [9] also documented optimized design for surface to point flow in conduction. However, there is a spacing between the tip of pathway and low conductivity material as shown in Figure 3.

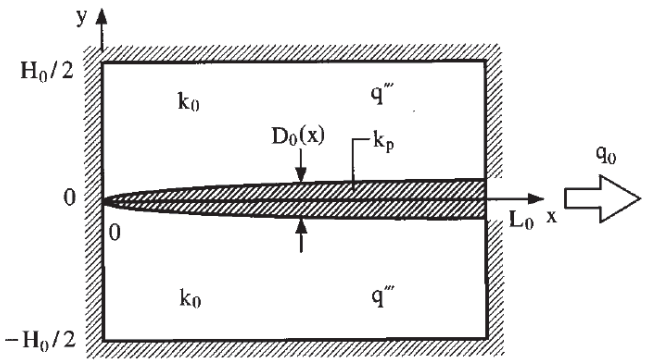

Figure 2. Variable diameter high-conductivity pathway in a heat generating volume [8]

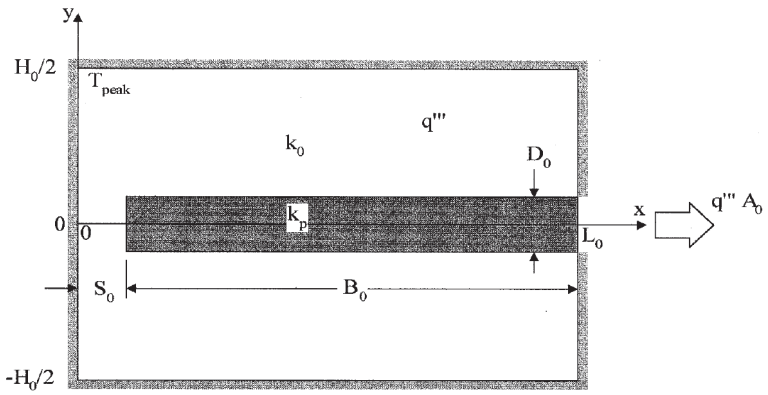

Figure 3. High-conductivity pathway with spacing [9]

They documented optimum thickness of pathway and optimum number of branches. When external shape become slender, T_{max} becomes lower. In addition, they indicated that spacing in between the low conductivity material and the tip of pathway decreases the maximum temperature by 20 %

Lorenzini et al. [10] optimized the non-uniform X-shaped conductive pathways in a heat generating domain, Figure 4. The optimization parameters are L_1/L_0, L_2/L_0, α and β. The results show that β_{opt} is function of $\tilde{k}_p\phi$ where $\tilde{k}_p$ is the dimensionless thermal conductivity and ϕ is the volume fraction of X-shaped pathway. α_{opt} is a negative value. In addition, optimum L_2/L_0 is a function of α_{opt}. There is an optimum value for L_1/L_0. $(L_1/L_0)_{opt}$ leads to significant increase in α_{opt}. After optimized non-uniform X-shaped pathway, it was compared with optimized uniform X-shaped pathway. Comparison result shows that optimized non-uniform X-shaped pathway decreases the

thermal resistance in the domain 56 % more than optimized uniform X-shaped pathway, Figure 5.

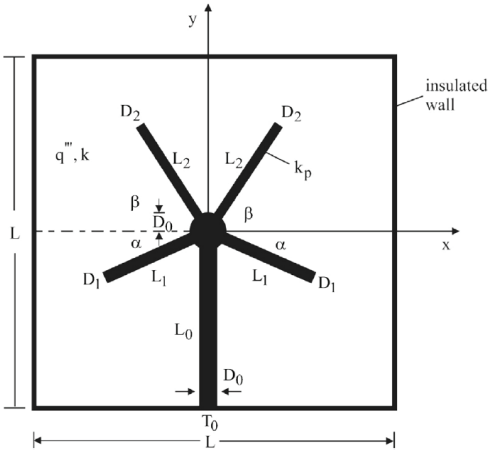

Figure 4. Non-uniform X-shaped pathway in heat generating domain [10]

Hajmohammadi et al. [11] documented the optimized fork-shaped pathways to minimize thermal resistance. They used two different types of fork-shaped high conductivity pathways, Figure 6. The optimization parameters for Figure 6a are H_1/H, e/H, D_2/H_2, D_0/H_0 and ω (volume fraction of high conductivity pathways).

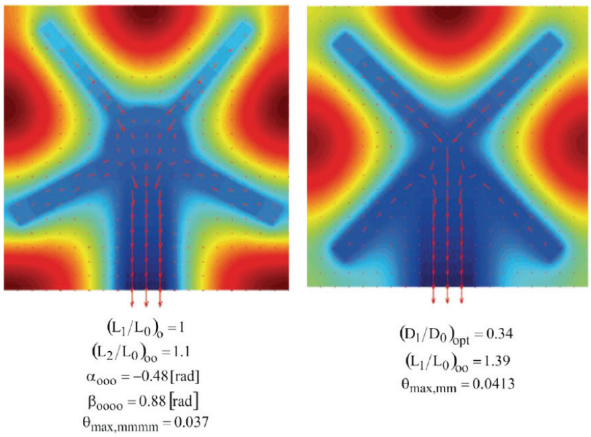

Figure 5. (a) Optimized non-uniform X-shaped pathway; (b) Optimized uniform X-shaped pathway [10]

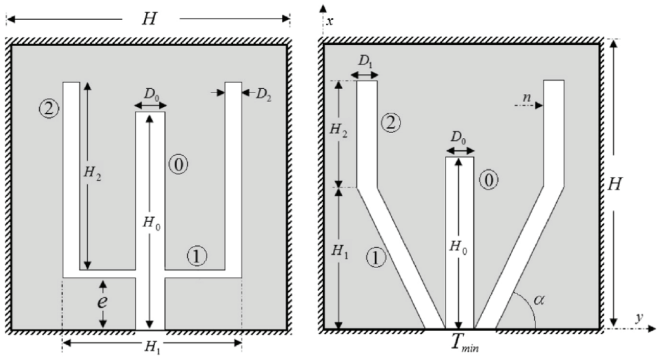

Figure 6. Geometry of high conductivity pathways [11]

The results for the design of Fig. 6a show that $(H_1/H)_{opt}$ increases when e/H increases. $(e/H)_{opt}$ varies with D_2/H_2. In addition, T_{max} decreases as ω increases. The optimization parameters of design in Figure 6b are the same with Fig. 6a with an additional parameter of α. α_{opt} increases when D_1/H_1 is increased. $(D_0/H_0)_{opt}$ does not change with ω. However, $(D_1/H_1)_{opt}$ increases as ω increases. Furthermore, they showed that the fork-shaped high conductivity pathways decrease T_{max} greater than X-shaped and I-shaped pathways for the same thermal conductivity (λ) and ω, as shown in Figure 7.

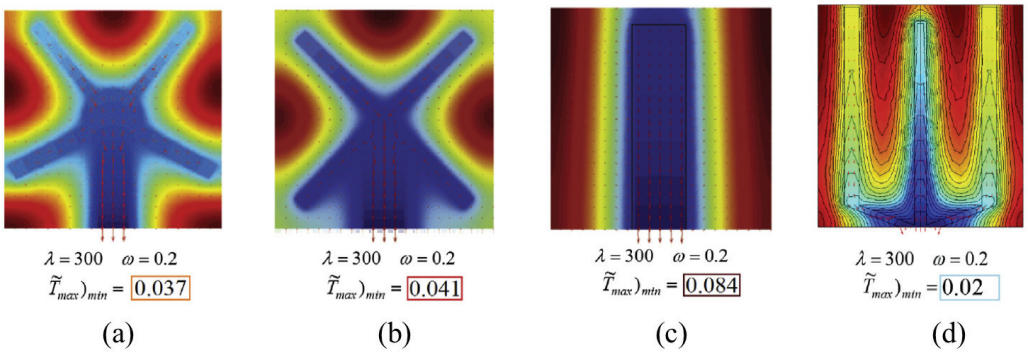

Figure 7. Comparison of optimized X-shaped, I-shaped and fork-shaped pathways [11]

Hajmohammadi, et al. [12] optimized Phi and Psi shaped pathways to decrease T_{max} in a heat generating domain which is shown in Figure 8. Optimization results for phi-shaped indicate that $(H_r/H)_{opt} \approx 0.51$, i.e., the configuration should be located at the centre of the domain. T_{max} decreases with increasing ω_r (volume fraction of ring

shaped of the insert), and there is an optimum ω_r. In addition, there is an $(H_r/H)_{opt}$ for psi-shaped, and T_{max} decreases as ω_s (volume fraction of stem shaped of the insert) decreases.

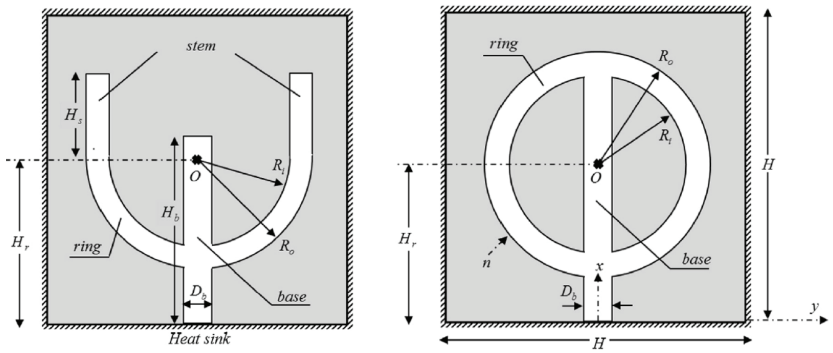

Figure 8. (a) Phi-shaped insert; (b) Psi-shaped insert [12]

Horbach et al. [13] used Y-shaped high conductivity pathways to enhance heat transfer for a volumetrically heat generating domain. The aim is to reduce T_{max} considering Constructal theory. The heat generating domain is a square, and it includes Y-shaped pathway, as shown Figure 9. The optimization parameters are α, L_1/L_0, D_1/D_0 and $\widetilde{D}_0$.

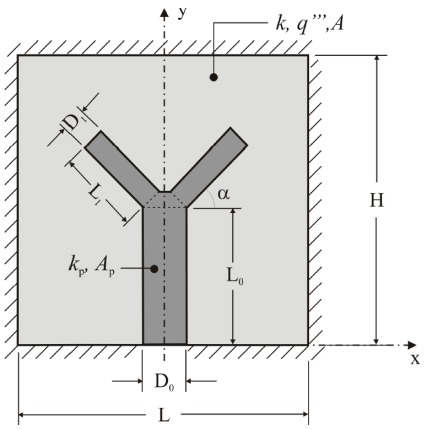

Figure 9. Y-shaped pathway in heat generating domain [13]

The optimization results show that there is $(L_1/L_0)_{opt}$ is equal to 4, and it increases as α increases. They documented that α_{opt} is 70°, and $(D_1/D_0)_{opt}$ is 0.5. $(\widetilde{D}_0)_{opt}$ is 0.14 for the domain. In addition, effect of thermal conductivity was analyzed

in the study. They used dimensionless thermal conductivity (k_p) in between 30 and 120. ΔT_{max} continues to decrease until k_p increases up 250. After that point, ΔT_{max} becomes insensitive to k_p. Furthermore, k_p affects optimum geometric values. When k_p increases, optimized L_1/L_0 and α_{opt} increase as shown in Fig. 10. This result also uncovers that when k_p is increased, optimum geometry corresponds to V-shaped.

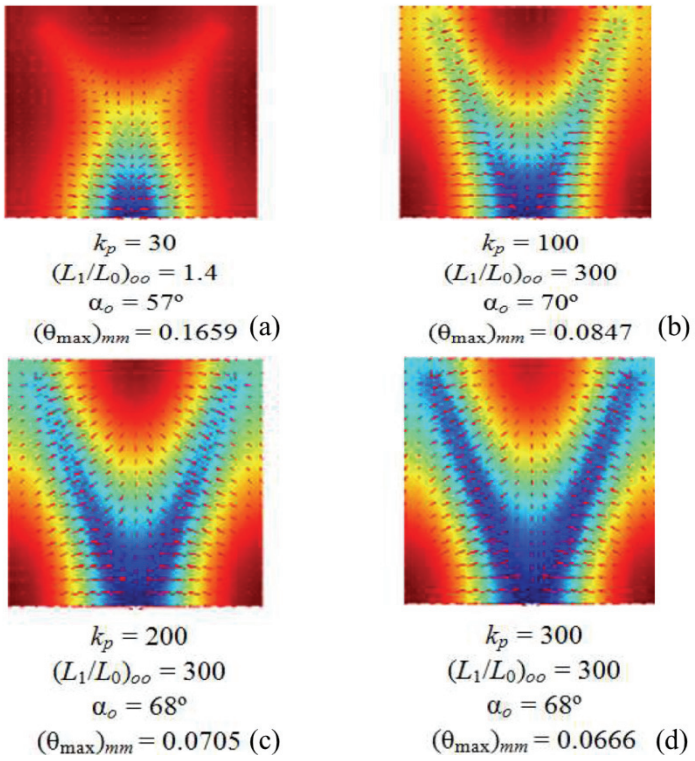

Figure 10. Optimized configurations for different k_p [13]

Hajmohammadi et al. [14] uncovered optimized V-shaped high conductivity pathways considering Constructal theory. They had two-dimensional heat generational domain with high conductivity pathways, Fig. 11. There are four geometries for optimization, which were used for optimization, respectively. The parameters were separately defined for each geometry. $(D_i/H_i)_{opt}$ and α_{opt} were documented for V1. Optimum D_i/H_i and D_m/H_m were uncovered for V2. For V3 optimum ω_a (volume fraction of auxiliary pathways) was documented, which affects optimum D_i/H_i in V3. For V4 optimum ω_a and optimum ω_m (volume fraction of middle pathways) increase as ω increases. In addition, optimized D_i/H_i and D_m/H_m increase when ω increases. The

optimized V-shaped pathways are shown in Fig. 12 for constant λ (thermal conductivity) and ω (total volume fraction of high-conductivity pathways).

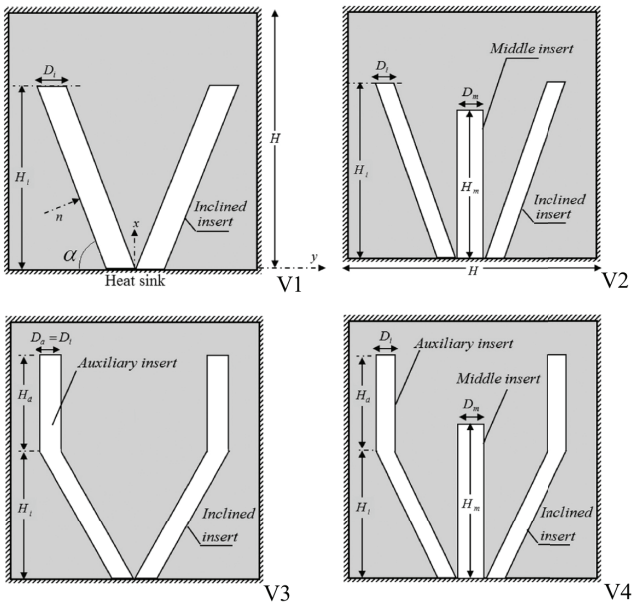

Figure 11. Geometry of high conductivity pathways [14]

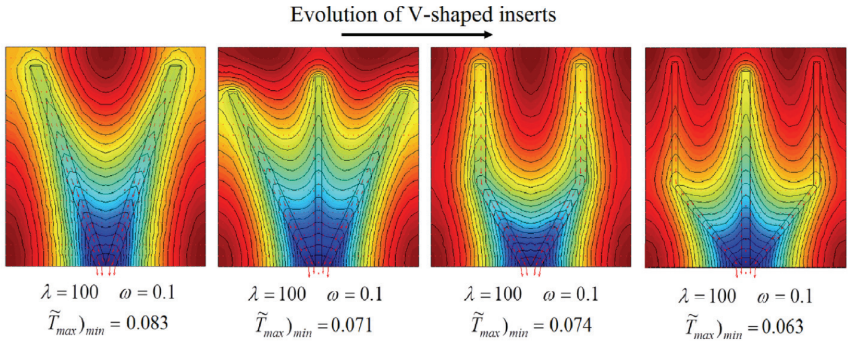

Figure 12. Optimized configurations of V-shaped pathways [14]

Huijun et al. [15] optimized design of "+" shaped high conductivity pathways in a heat generating domain, Fig. 13. They optimized the system for both single and multilevel "+" shaped high conductivity pathways with Constructal Theory. They optimized dimensionless D_0 ($\widetilde{D}_0$) for single "+" shaped high conductivity pathways. For multilevel "+" shaped high conductivity pathways, optimization parameters are D_1/D_0, L_1/L_0 and $\widetilde{D}_1$(dimensionless D_1). Because of symmetry, Figure 13a and Figure 13b were used as optimized domains.

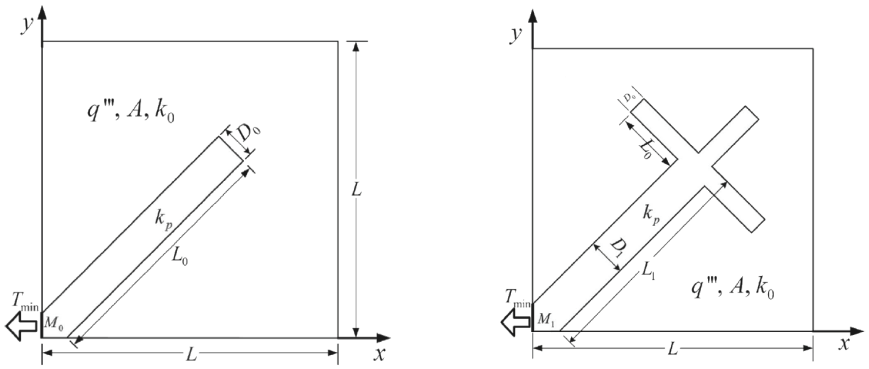

Figure 13. (a) Single "+" shaped high-conductivity pathways; (b) Multilevel "+" shaped high-conductivity pathways [15]

The result for single "+" shaped high conductivity pathways show that optimum $\widetilde{D}_0$ varies depending on $\tilde{k}$ (dimensionless thermal conductivity). When $\tilde{k}$ increases, $\widetilde{D}_0$ decreases. Furthermore, optimization of multilevel "+" shaped high conductivity pathways results show $(D_1/D_0)_{opt}$, $(L_1/L_0)_{opt}$ and $(\widetilde{D_1})_{opt}$. The effect of $\tilde{k}$ was also analyzed for them. $\tilde{k}$ does not significantly affect the $(\widetilde{D_1})_{opt}$ and $(L_1/L_0)_{opt}$. However, $(D_1/D_0)_{opt}$ decreases when $\tilde{k}$ increases until a certain $\tilde{k}$ value. In addition, the optimized configuration of multilevel "+" shaped high conductivity pathways were compared to optimized X-shaped pathways. Comparison in Figure 14 indicates that the thermal resistance is decreased by multilevel "+" shaped high conductivity pathways 75.79 % greater than X-shaped pathways.

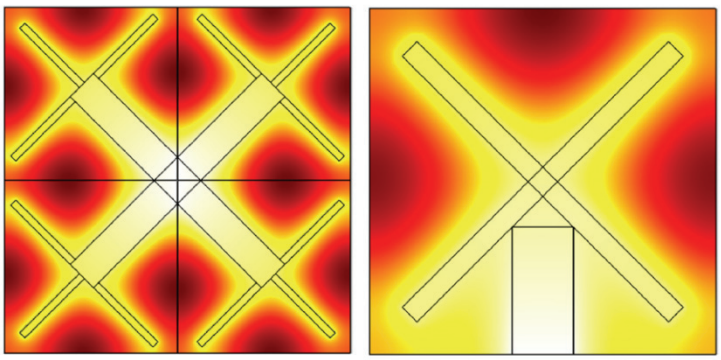

Figure 14. (a) Multilevel "+" shaped high conductivity pathways and (b) X-shaped pathways [15]

Cetkin and Oliani [16] analyzed formation of asymmetric tree-shaped pathways for a cooling of a non-uniformly heat generating domain, Figure 15. Firstly, they optimized the design when the heat generation is uniform and constant. They documented that T_{max} decreases when volume fraction of high-conductivity pathways (ϕ) and the number of bifurcation (N) increases. Then, they considered the non-uniform heat generation, and its effect was obtained from 3 distinct points. Maximum T_{max} is observed heat generation location where is the farthest from both heat sink and conductive pathways. For the non-uniform heat generation condition when N increases, the effect of heat generation location diminishes. Then, they used Y-shaped fins in order to obtain asymmetric high conductive pathways as shown in Figure 16. They uncovered that the formation of pathways tends to where heat generation occurs.

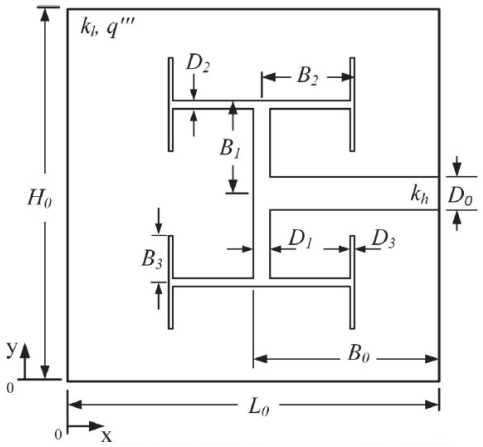

Figure 15. Heat generating domain with high conductive pathways [16]

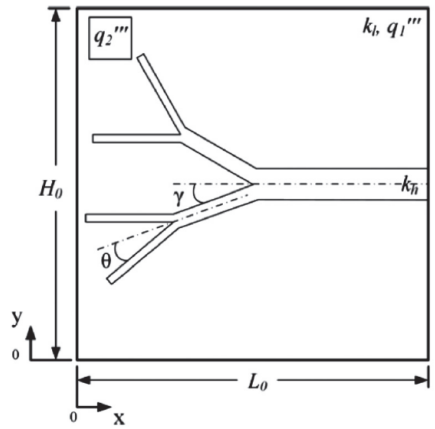

Figure 16. Heat generation domain with asymmetric Y-shaped pathways [16]

Eslami [17] optimized analytically pencil shaped (V-shaped) geometry for only rectangular heat generating domains, Fig. 17. The optimization parameters are n (the number of link), H/L and φ (volume fraction of high-conductivity material).

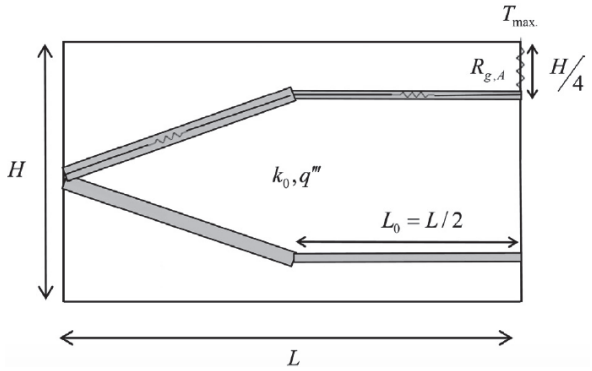

Figure 17. Pencil shaped elemental volume [17]

The results show that when n increases, R_g (thermal resistance of pencil shape design) decreases, but R_1 (thermal resistance of links) increases in Figure 18. Therefore, n_{opt} was uncovered to decrease thermal resistance. $n_{opt} = \hat{k}\varphi$, where $\hat{k}$ is the dimensionless thermal conductivity. Optimum φ for each link nearly equals to $0.5 \times \varphi$ for this domain. In addition, Eslami uncovered that $(H/L)_{opt}$ is a universal constant, and it is equal to 2.

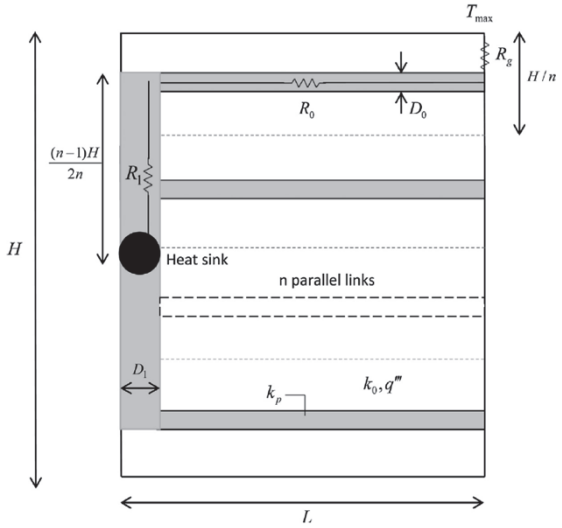

Figure 18. The parallel design [17]

Lorenzini et al. [18] uncovered the effect of the thermal contact resistance on optimization of geometry between an I-shaped high-conductivity pathway and low conductivity material, Fig. 19. The parameters of optimization are H_0/L_0 and H/L. They documented that the effect of thermal contact resistance becomes more sensible as the conductivity of high thermal conductivity material increases. In addition, thermal contact resistance affects the optimum parameters. When thermal contact resistance ($\tilde{k}_L$) decreases, optimum parameter decreases, but ΔT_{max} increases, as shown in Figure 20.

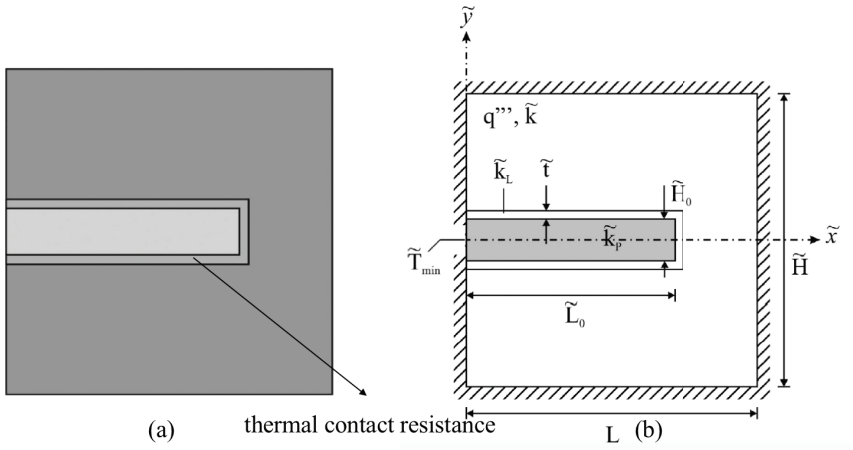

Figure 19. (a) The geometry used in numerical simulation; (b) Conductive material with thermal contact resistance with heat generation [18]

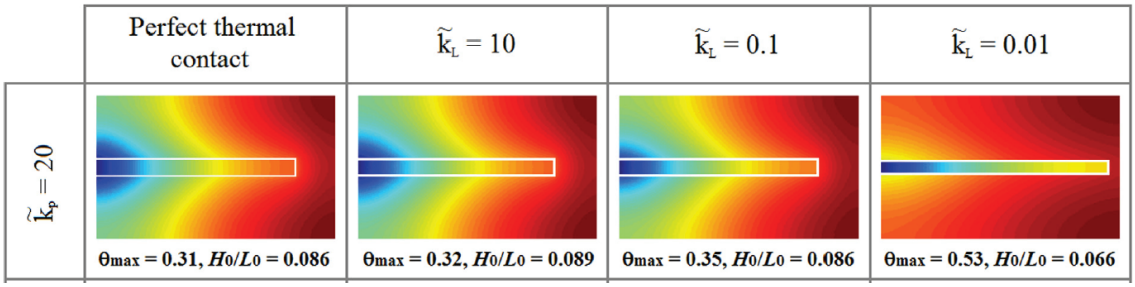

Figure 20. Optimized configurations for perfect condition and different thermal contact resistance values [18]

In other study Lorenzini et al. [19] demonstrated the effect of thermal contact resistance between T-shaped fin and heat generating domain, which is shown in Figure 21. They numerically optimized the geometry based on Constructal theory in order to reduce T_{max}. L_1/L_0 and D_1/D_0 were optimized for both the presence of thermal resistance and the perfect thermal contact situation.

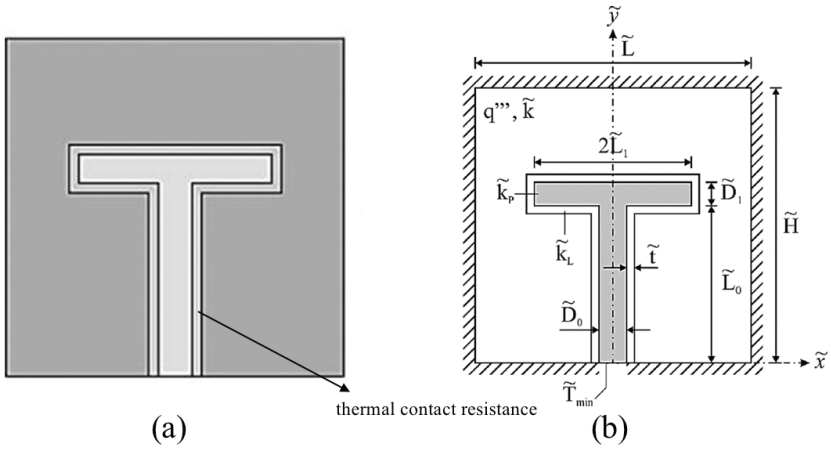

Figure 21. (a) The geometry with third element used in numerical simulation; (b) The geometry with thermal contact resistance in the domain [19]

The results showed that thermal contact resistance affects the global thermal resistance significantly. They found that $(L_1/L_0)_{opt}$ is less if thermal contact resistance exists, Figure 22. Similarly, $(D_1/D_0)_{opt}$ decreases in the presence of thermal contact resistance. It resulted an increase in the global thermal resistance by 25 % compared to the ideal situation in which thermal contact resistance is ignored.

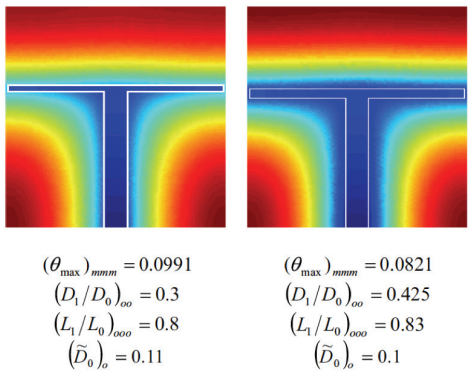

Figure 22. (a) Model with thermal contact resistance; (b) Model with perfect thermal conduct situation [19]

Jiang et al. [20] optimized high-conductivity pathways in a non-uniform triangular heat generating domain, Fig. 23a. They separately used constant and variable cross-sectional high conductivity pathways in the domain. During the optimization, the top of the domain ($x = L_0$) was ignored, which is shown Fig. 23b. They defined p as the coefficient of non-uniform heat generation. In order to optimize, the external

shape, H_0/L_0 parameter was used. In addition, D_1/D_0 and H_1/L_1 are the parameters for optimization of the first order assembly, Fig. 24a.

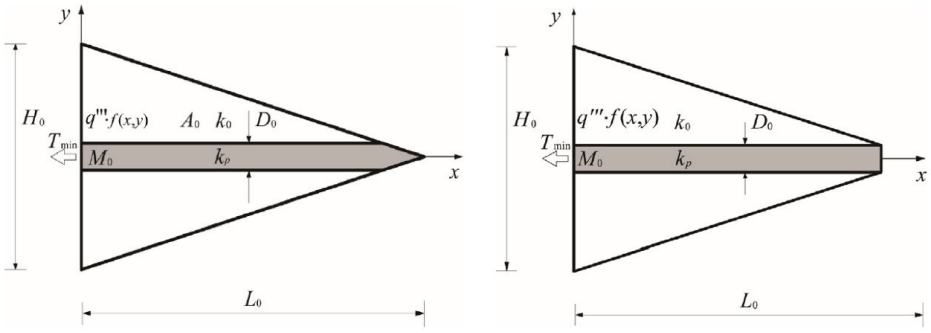

Figure 23. (a) Triangular element with non-uniform heat generation; (b) Triangular element with non-uniform heat generation ignoring heat transfer at the top [20]

The optimization result for external shape indicates that $(H_0/L_0)_{opt}$ depends on the value of p. As p increases, $(H_0/L_0)_{opt}$ decreases. In addition, the results of the first assembly show that p affects the $(D_1/D_0)_{opt}$ and $(H_1/L_1)_{opt}$. Furthermore, if the high conductivity pathways have discrete variable cross-sectional, Fig. 24b, additional parameters exist, such as D_{11}/D_{12}, D_{12}/D_{13} and D_{13}/D_0. p also affects $(D_{11}/D_{12})_{opt}$, $(D_{12}/D_{13})_{opt}$ and $(D_{13}/D_0)_{opt}$. Moreover, discrete variable cross-sectional high-conductivity pathways decrease minimum ΔT_{max} 12. 57 % more than constant high-conductivity channels as shown in Fig. 25.

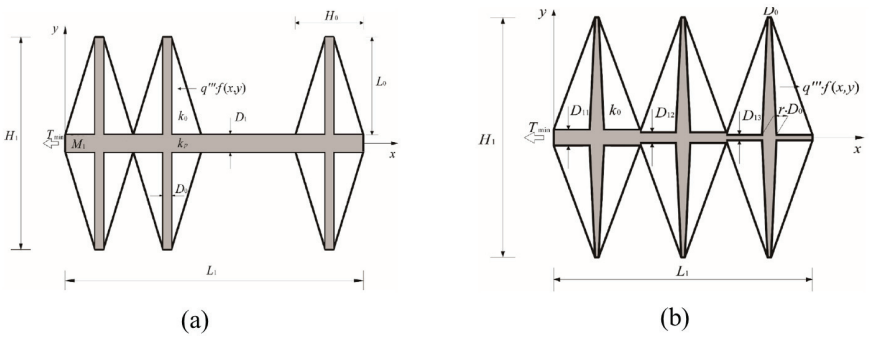

Figure 24. (a) Geometry of constant cross-sectional pathways; (b) Geometry of discrete variable cross-sectional pathways [20]

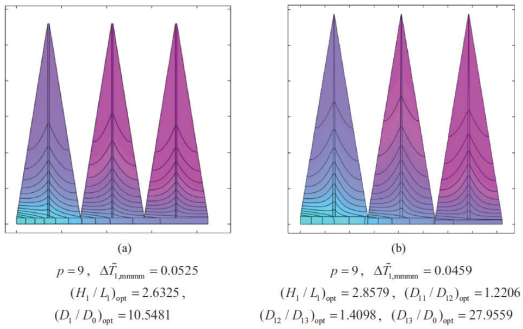

Figure 25. (a) Optimized geometry with constant cross-sectional high-conductivity pathways; (b) Optimized geometry with variable cross-sectional high-conductivity pathways [20]

1.2. Fins

Biserni et al. [21] documented the optimization of cavity (inverted fins) shape for two-dimensional domain as shown in Figure 26 based on Constructal Theory. They used C-shaped conducting body for two conditions. In the first condition heat is volumetrically generated in the domain. They optimized C-shaped configuration numerically. There are three parameters for optimization, which are H/L, H_0/L_0 and ϕ (H_0L_0/HL).

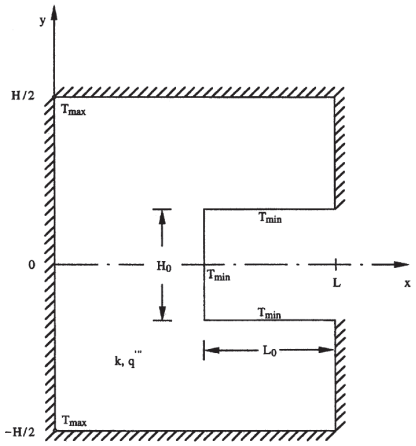

Figure 26. Conducting domain with uniform heat generation [21]

The results indicate that when ϕ increases, the thermal resistance decreases. In addition, there is no optimum value for H/L whereas optimum H_0/L_0 exists. In the second condition the C-shaped is heated with uniform heat flux (q'') externally, and the internal heat generation does not exist, Fig. 27. For this condition, firstly, optimum H_0/L_0

was documented. Secondly, they found out that the thermal resistance increases with increase in H/L, and there is no optimum H/L .

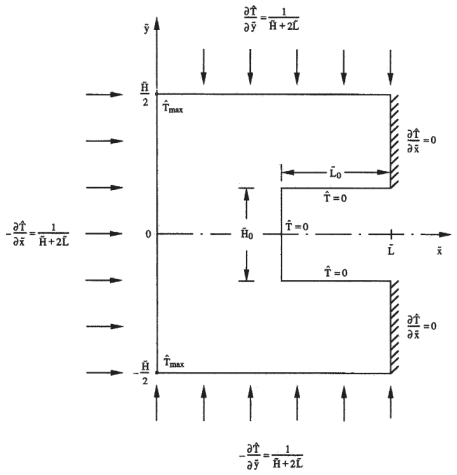

Figure 27. Domain with uniform heat flux on its external surface [21]

Figure 28 shows the T-shaped construct. For optimum tree-shaped construct L_0/L_1, H/L and D_0/D_1 are the parameters. $H/L = 1$ and it was fixed.

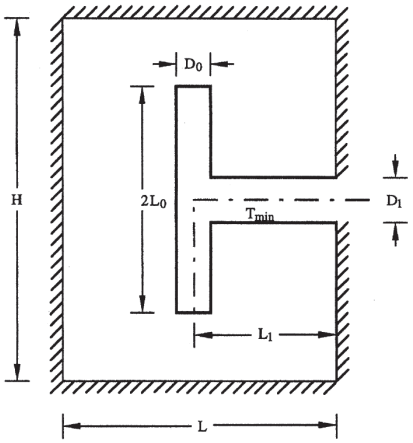

Figure 28. T-shaped assembly in the body [21]

The results indicate that optimum L_0/L_1 does not depend on D_0/D_1. In addition, there is no optimum value for D_0/D_1. The global resistance and optimum lengths decrease while ϕ (volume fraction of cavity) increases. In addition to ϕ effect, the effect of ψ (volume fraction of T-shaped construct) was analyzed. They stated that while ψ increases,

the thermal resistance decreases, but optimum L_0/L_1 increases at the same time, in Fig.29.

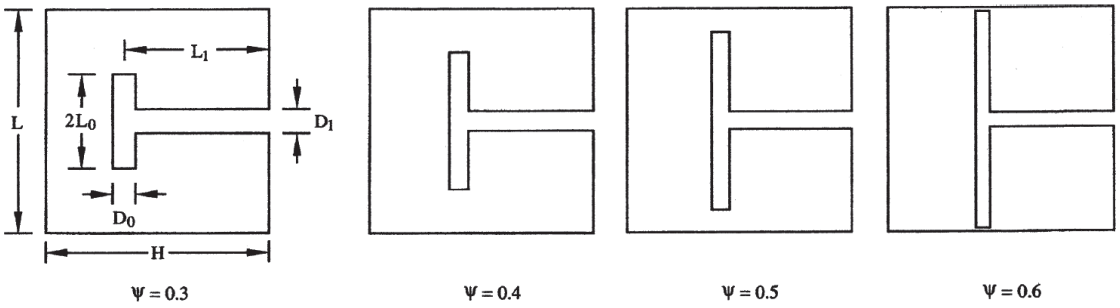

Figure 29. The optimum configurations when 0.3 < ψ < 0.6 [21]

Lorenzini and Rocha [22] analyzed the Y-shaped fins numerically. Their aim is to minimize the global thermal resistance according to Constructal theory. They used three parameters, which are L_1/L_0 , t_1/t_0 and α, Fig. 30. The results show that t_1/t_0 is not important parameter for optimization. Otherwise, optimum α increases very slightly when t_1/t_0 increases. Moreover, while L_1/L_0 increases, optimum α and maximum temperature difference decreases. In addition, they stated that Y-shaped fins decreases thermal resistance nearly 11 % better than T-shaped fins.

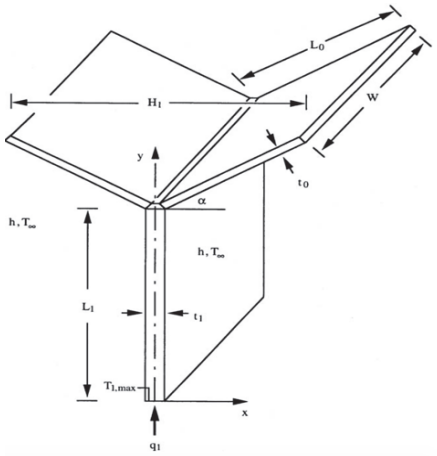

Figure 30. Y-shaped assembly of fins [22]

Lorenzini and Moretti [23] optimized Y-shaped fins numerically and studied on performance of Y-shaped fins optimization based on T-shaped fins, as show in Figure 31. They analyzed heat transfer mechanism, the effect of the angle α between the arms of T-

shaped, and they reached Y-shaped fin profile. There are 3 conditions for optimization. They are $180 < \alpha < \alpha_{lim}$, $\alpha_{lim1} < \alpha < 180$ and $\alpha_{lim3} < \alpha < \alpha_{lim2}$ as shown in Figure 32.

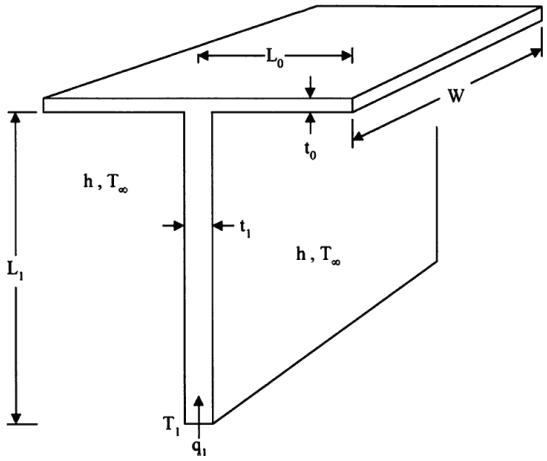

Figure 31. T-shaped fin used for optimization [23]

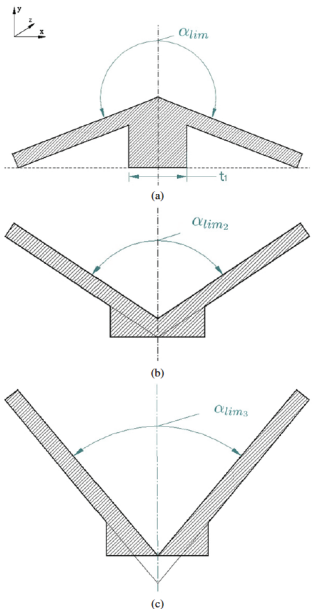

Figure 32. Geometry cases I (a), II (b), III (c) [23]

They observed that L_0 is independent from angle α, Fig. 33. In addition, they showed that the effect of the angle α between the arms of T-shaped on geometric optimization, and they reached Y-shaped fin profile as an optimum configuration derived from T-shaped fin.

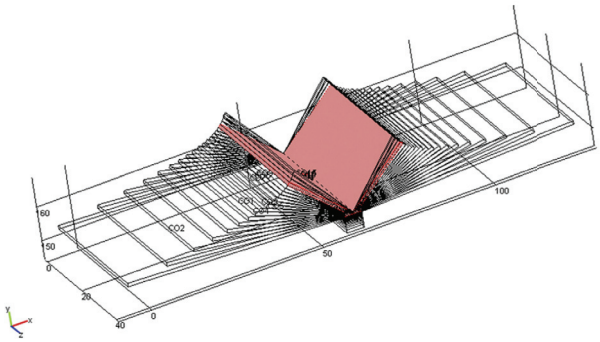

Figure 33. The geometry independent from α [23]

Xie et al. [24] numerically optimized twice Y-shaped assemblies of fins. The geometric parameters are α, β, t_2/t_1, t_1/t_0, L_2/L_1 and L_1/L_0, as shown in Figure 34. The results show that increase in $(L_1/L_0)_{opt}$ causes decrease in α_{opt}. However, if $(L_1/L_0)_{opt}$ increases, maximum thermal resistance and β_{opt} increase. Similarly, increase in L_2/L_1 leads to increase in maximum thermal resistance. In addition, the effect of t_2/t_1 and t_1/t_0 on the thermal resistance is much smaller than the effect of L_2/L_1 and L_1/L_0. Moreover, they explained that twice Y-shaped assemblies transfers heat 36.37 % better than once Y-shaped fin assembly.

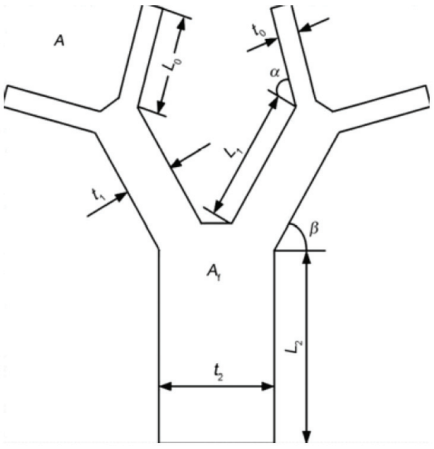

Figure 34. Twice Y-shaped fin assemblies [24]

Lorenzini et al. [25] optimized T-shaped assemblies of fins in a cylindrical solid body where heat is generated. Conductive heat transfer and convective heat transfer exist in the domain. The parameters of optimization are L_1/L_0 and t_1/t_0. In addition, they analyzed the effect of the number of fins, as shown in Figure 35.

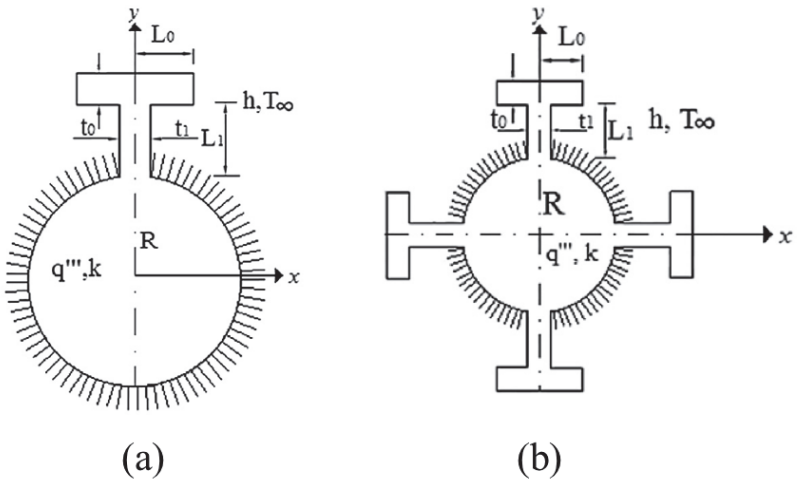

Figure 35. (a) Computational domain; (b) Computational domain for 4 fins [25]

The optimization results show that there is an optimum value for L_1/L_0, but it is so small. If it is increased, the ratio becomes more dominated. Otherwise, while L_1/L_0 changes, there is no general geometry for minimum ΔT_{max}. In addition to them, minimum ΔT_{max} and $(t_1/t_0)_{opt}$ decrease if L_1/L_0 increases. It is demonstrated that T-shaped fins work better when they become slender while the stem becomes thicker because of existing more number of freedom. In addition, when the number of fins assemblies are increased, minimum ΔT_{max} decreases. It indicates that the geometry of the fins is variable depending on their number.

Cetkin [26] stated that how T_{max} is reduced with T-shaped inverted fins embedded in a non-uniformly heat generating domain, Figure 36. The optimization parameters are d_2/d_1, d_3/d_1, d_4/d_1, d_5/d_1, d_6/d_1 and d_7/d_1. In addition, Cetkin analyzed the effect of bifurcation and Y-shaped fin. The results show that when there is no bifurcation, if φ (volume fraction of fin) increases, T_{max} decreases. There are optimum d_2/d_1 and d_3/d_1. In addition, location of hot spot affects $(d_2/d_1)_{opt}$ and $(d_3/d_1)_{opt}$. When bifurcation level is increased, T_{max} decreases. In addition, T_{max} decreases as d_4/d_1 and d_6/d_1 decrease. Furthermore, the result of Y-shaped fin shows that it decreases T_{max} greater than T-shaped fin.

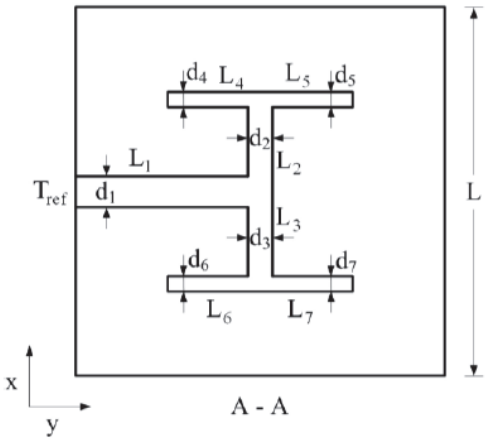

Figure 36. High-conductivity tree embedded in the domain [26]

Huijun et al. [27] analyzed numerical optimization of helm-shaped fins according to Constructal Theory. Their domain consists of three-dimensional helm-shaped fin with a number of (n) internal heat sources. The fin consists of one cylinder and a number of (N) sectorial extended bodies with an angle α, shown in Figure 37.

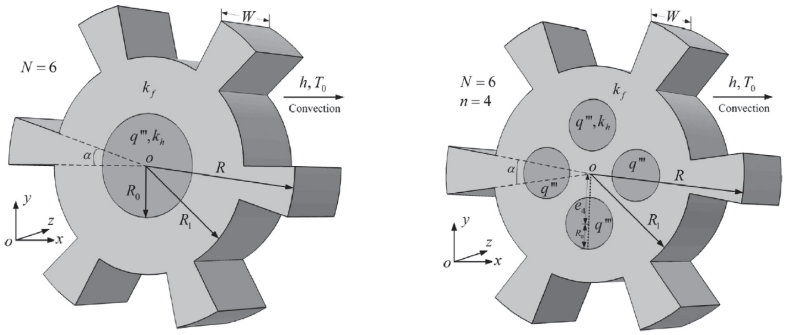

(a) (b)

Figure 37. (a) Helm-shaped fin with one internal heat source; (b) Helm-shaped fin with 4 internal heat sources [27]

Volume fraction of internal heat sources (ϕ_0) and volume fraction of helm-shaped fins (ϕ_1) are the constraints. The optimization results show that when n = 1, the dimensionless thickness ($\widetilde{W}$) of the fins should not be 0.33. In addition, thermal resistance decreases when ϕ_1 increases, and N decreases. When n > 1, the system has double thermal resistance. In addition, multiple internal heat sources and non-uniform heat generation provide better systems for helm-shaped fins. Therefore, optimum number of internal heat sources should be documented for minimum thermal resistance.

1.3. Snowflake Formation

People are always interested in the snowflake shape. William Bentley is the first person to take pictures of snowflakes. He had 5,000 snowflake images at that time. In 1951 scientists created a classification system in International Association of Cyrospheric Science. They had 10 different snowflake shapes, which is shown in Figure 38. Today scientist still use this method, and they develop new methods [28]. Kihuchi et al. [29] launched a new classification catalog that includes 121 classes for snow crystal and solid precipitation particles. These classes were constituted with observations from middle latitudes to polar regions. They classified aggregation of snow crystals in the 3 intermediate groups, which are aggregation of column-type crystals, plane- type crystals and column- and plane- type crystals. They stated that the reason of different type of crystals is temperature difference at different altitudes.

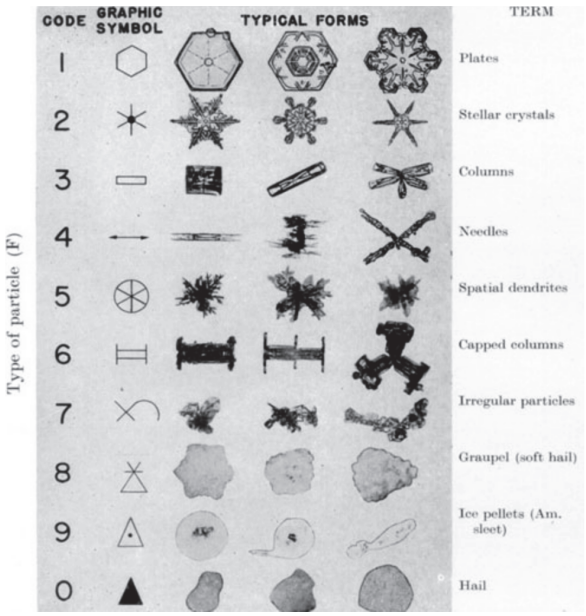

Figure 38. Classified snowflake shapes in 1951 [28]

On the other hand, nowadays scientists create new models in order to understand snowflake formation. Tyynela et al. [30] made simulations for physical properties of real snowflakes, which are mass-size relation and aspect ratio. They stated that different ice crystal habits lead to the variable mass-diameter relation, which results in formation of different cross sections for different sizes. In addition, aspect ratio is defined the ratio of maximum vertical extent in z direction and maximum horizontal extent in x and y

directions. By using the definition, they estimated that aspect ratio is 0.65, and it is coherent with real measurement in the literature. In other study, Nowell et al. [31] simulated the formation by using a different approach than Tyynela et al. [30]. They used six-bullet block "rosette" as the constitute particles in the study as shown in Figure 39a. They aggregated the snowflake shape as shown in Figure 39b. They explained that the shape of aggregation can vary depending on temperature, water concentration, collision of particles and their fall speed. In addition to snowflake shape formation studies, some researchers use snowflake shapes for developing systems. For instance, Lee et al. [32] used three-dimensional snowflake shape for webs of carbon fibers. Their aim is to increase performance of cathode material of lithium batteries. The results show that the snowflake shape form provides good cycling stability and high discharge capacity for lithium batteries.

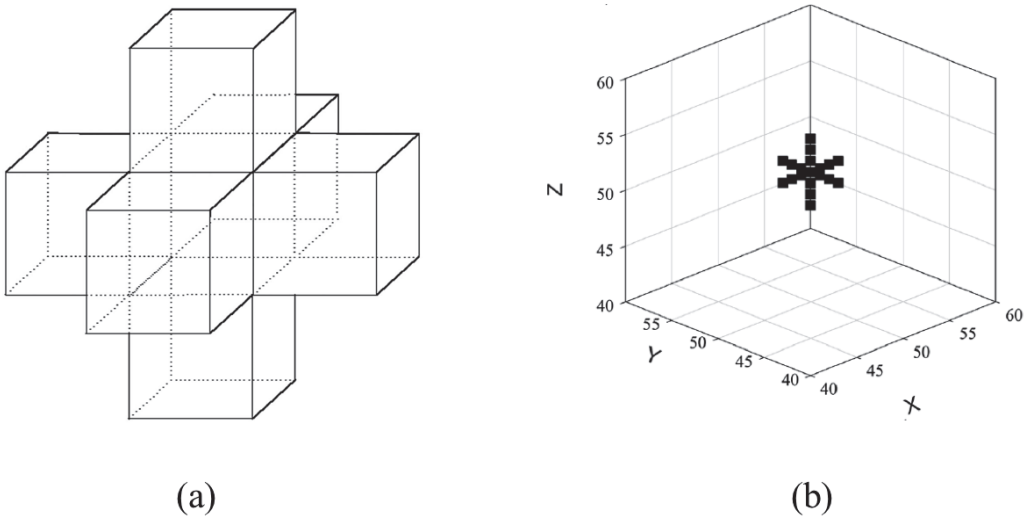

Figure 39. (a) Six-bullet block "rosette" as the constitute particles; (b) A single rosette crystal [31]

In addition, Albanese et al. [33] designed snowflake-shaped magnetic tokamak configurations in order to increase fusion power and to decrease maximum heat load. They had good results with snowflake-shaped configuration in some type of tokamaks, and they still study on other tokamak types.

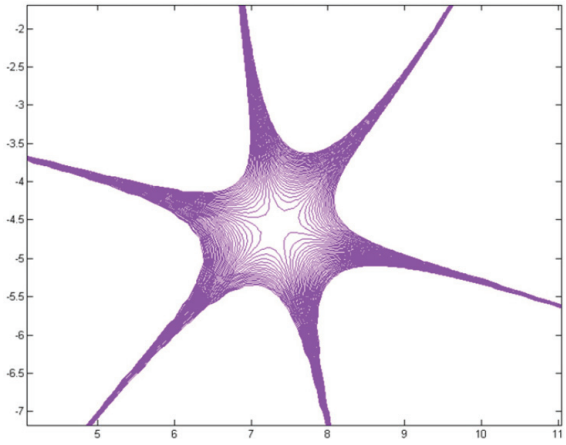

Figure 40. The configuration of snowflake shaped divertor tokamak [33]

In this thesis, we document the optimum fin shape to minimize thermal resistance in between a point source and a conducting surface. The volume of fins was fixed, and the thermal resistance was decreased with only varying the design depending on Constructal law. The optimized design which is corresponding to the minimum thermal resistance is similar to a specific type of a snowflake. We documented optimum number of mother and daughter fins, their locations, their dimensions, and fin angle in the domain to obtain minimum T_{max}. Here, the design was not dictated as the design of snowflake as literature focuses. The design is free to evolve, and it evolves to a snowflake design to minimize the resistance to its flow (i.e., heat).

CHAPTER 2

MODEL AND METHODS

2.1. Model

Consider a two-dimensional domain where heat is generated by a point heat source, the size of $\pi \times R^2$. The heat is generated with constant heat flux, q''. The external shape of the domain is a square with the scale of L. In the domain there are high conductivity pathways, which are fins, in order to control T_{max}. The fins with high thermal conductivity k_h are rectangular which are embedded around the heat source. The rest of the domain is composed of low conductivity material with low thermal conductivity k_l. The area of external shape (A_s) is fixed. Otherwise, fin area (A_f) and fin ratio (t_f/L_f) may change. A constant surface temperature, T_{sur}, exist for outer surface of the square domain with length scale of L. The other boundary condition is constant surface heat flux ($\partial T/\partial \theta = q''$) at the circle surface.

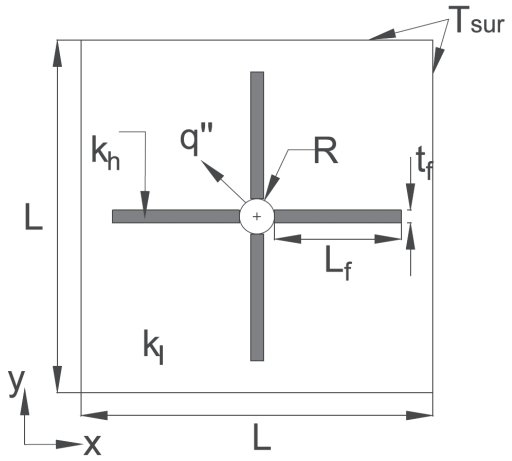

Figure 41. The general view of the domain

In addition to them, for the sake of simplicity heat transfer occurs in the steady state. The materials are isotropic with constant material properties. With this in mind, the

heat transfer energy equations were solved simultaneously by using a finite element software, COMSOL Multiphysics 5.0 [34], respectively.

$$k_l\left(\frac{\partial^2 T}{\partial x^2}+\frac{\partial^2 T}{\partial y^2}\right)=0 \tag{2.1}$$

$$k_h\left(\frac{\partial^2 T}{\partial x^2}+\frac{\partial^2 T}{\partial y^2}\right)=0 \tag{2.2}$$

The heat flux continuity between high and the low conductivity material is,

$$k_l\left(\frac{\partial T}{\partial n}\right)=k_h\left(\frac{\partial T}{\partial n}\right) \tag{2.3}$$

where n is the normal vector to the interface of high and the low conductivity material.

2.2. Method

Consider radius of the point heat source is 0.01 m with 1W/m^2 heat flux. The length of the square is 1 m with T_{sur} = 273.15 K, and the area of the square domain was fixed through the text, so is the area fraction of fins. Thicknesses and lengths were calculated depending on number of fins and volume fraction. Area fraction (ϕ) is the ratio of fin area divided by the area of square domain.

$$\phi=\frac{A_f}{A_s}=\frac{m\times L_f\times t_f}{L\times L} \tag{2.4}$$

where *m* is the number of fins.

Firstly, there are four symmetrical placed equilaterals spacing at the perimeter of the heat source of radius 0.01 m, while $t_f/L_f=0.1$ and ϕ was varied in between 0.001 and 0.01.

Unstructured mesh with quadratic shape functions were used through the study. In order to uncover when the results become mesh independent, i.e. not a function of mesh size, mesh independency test was performed. The criterion is $\left|(T_{max}^{i}-T_{max}^{i+1})/T_{max}^{i}\right|<5\times10^{-6}$ for mesh dependency. Table 1 uncovers that the

criterion was satisfied with the mesh number becomes greater than 4000 for various volume fractions. Because the mesh is unstructured, even the mesh properties defined as the same, number of the mesh elements vary due to change in the area fraction.

Table 1. Mesh Independency Results

	ϕ	Number of elements	T_{max}[K]	Error
$\frac{t_f}{L_f} = 0.1$	0.001	1450	274.354550	-
		3476	274.357288	9.97953E-06
		5088	274.357348	2.18217E-07
	0.002	1474	274.218492	-
		2810	274.220093	5.83651E-06
		4960	274.220299	7.53896E-07
	0.004	1236	274.065818	-
		2810	274.067420	5.84307E-06
		4704	274.067530	4.00885E-07
	0.006	1092	273.973381	-
		1964	273.974989	5.86758E-06
		4048	273.975983	3.63006E-06

In order to validate current numerical approach, the results were compared with the results of published literature. Table 2 documents the results of Ref. [9] and the relative error between them. The relative error is less than 0.4 %. Therefore, the results in the current study are coherent with results in Ref. [9].

Table 2. Validation Test Results

k	T_{max} in Ref. [9]	T_{max} in current study	Relative Error (%)
10	0.374893	0.37607	0.313956
30	0.224812	0.22519	0.168140
100	0.157219	0.15744	0.140568
300	0.135924	0.13612	0.144198
1000	0.128236	0.12842	0.143485

CHAPTER 3

RESULTS AND DISCUSSIONS

3.1. The First Assembly

The first assembly corresponds to the design with only mother pathways attached to a heat source at the center as shown in Figure 41. The fins were placed with equal distance at the perimeter of heat source. Area fraction (ϕ) varied from 0.001 to 0.01, but fin ratio (t_f/L_f) was constant and equal to 0.1 in the simulations to obtain optimum number of mother fins. Figure 42 indicates that while increasing ϕ, T_{max} decreases for all numbers of fin number. However, 4 number of fins corresponds to greater T_{max} value than both 6 and 8 number of mother fins. This corresponds to first extremum where the spacing in between the fins is big enough to increase the thermal resistance in low conductivity domain. T_{max} value becomes the same for 6 and 8 number of mother fins when ϕ = 0.004, below that T_{max} is minimum with 8 fins and above that it is minimum with 6 fins. These results uncover the second extremum (the spacing in between fins is short enough for thermal boundary layer to overlap) with 8 number of mother fins after ϕ = 0.004. Here, we select the 6 number of fins as the optimal number of mother fins even though the thermal resistance is minimum with 8 fins when $\phi < 0.004$. The reasons of this are very small difference in between the T_{max} values for 6 and 8 fins when $\phi < 0.004$, and 6 number of fins correspond to the smallest T_{max} for the rest of the surveyed ϕ values. Therefore, the second level of branches will be inserted at the tip of 6 fins.

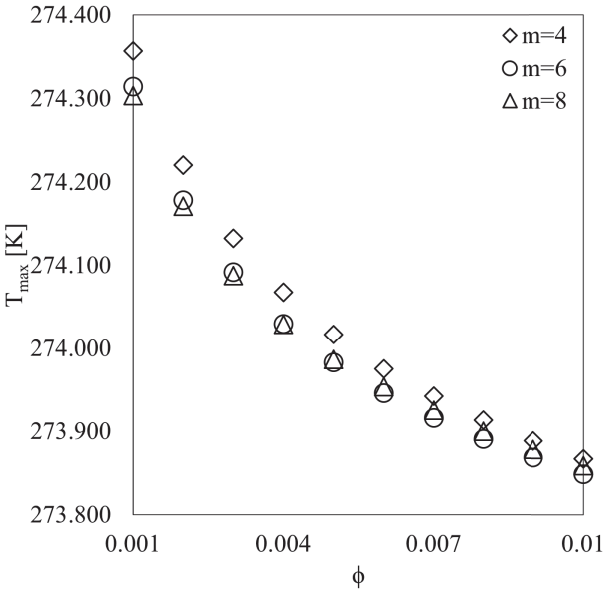

Figure 42. T_{max} relative to ϕ for various number of mother fins

3.2. The Second Assembly

3.2.1. Additional Branches

Figure 41 shows that in the first assembly high conductivity branches are connected with constant heat flux domain located in the center. The number of the identical branches and their area fraction affects the thermal resistance which inversely proportional to the T_{max} as shown in Figure 42. In addition, Bejan and Lorente [3] showed that thermal resistance can be minimized with addition of daughter (small) high conductivity pathways at the tip of mother (big) pathways for different boundary conditions and size. They have also uncovered the numbers of daughter channels should be more than the mother channels. Therefore, the effect of inserting additional pathways with relatively small thickness to the mother pathways was also discussed. The transition from one level of branch to two levels was uncovered, i.e. when the bifurcation should be. During all the studies the volume of the domains were fixed. In addition, the geometry was defined with three distinct fin ratios which are big fin ratio (BFR), small fin ratio (SFR) and fin ratio (FR). They are defined as:

$$BFR = \frac{t_b}{L_b} \qquad SFR = \frac{t_s}{L_s} \qquad FR = \frac{L_s}{L_b} \tag{3.1}$$

In the simulations of additional fins area fraction (ϕ) was constant, which was equal to 0.001. The lengths and thicknesses of fins are shown in Figure 43.

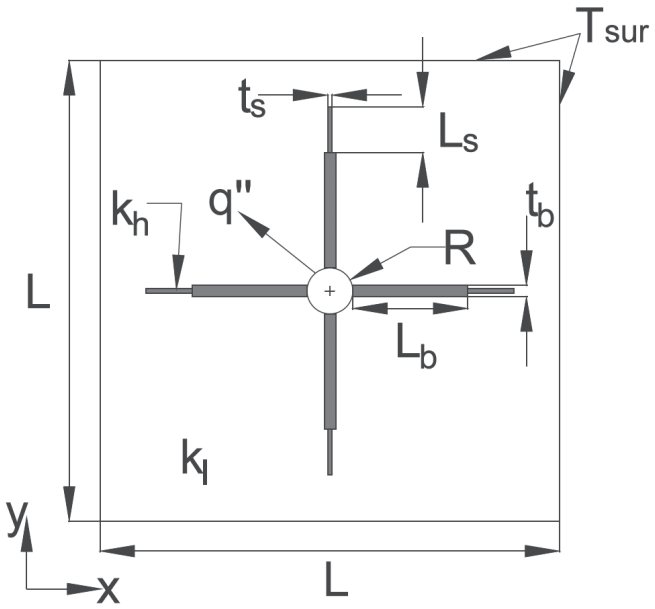

Figure 43. The domain with additional branches

3.2.2. One Daughter Fin Addition

After deciding optimum number of mother fins, for further reductions in thermal resistance, daughter (small) fins are attached to the tip of mother fins. In this assembly, one daughter fin was attached to the tip of each mother fins in the domain as shown in Figure 43. ϕ was 0.001, and it is fixed whereas the distinct fin ratios, BFR, SFR and FR, were free to vary. BFR and SFR were varied from 0.01 to 0.1, and FR were varied from 0.1 to 1. In addition to these, the optimization by using fin ratios were made according to a sequence, in which SFR_{opt} was found firstly with initial FR and BFR values as shown in Figure 44. Secondly, FR_{opt} was decided with SFR_{opt} and initial BFR value as shown in Figure 45. Lastly, BFR_{opt} was obtained with SFR_{opt} and FR_{opt}, as shown in Figure 46.

Figures 44, 45 and 46 show that there are optimum fin ratios for addition of one daughter fins. Here, Fig. 44 shows that SFR_{opt} is equal to 0.07. Fig. 45 shows that FR_{opt} is 0.3. In addition, Fig. 46 shows that BFR_{opt} is 0.02, and T_{max} is lower than T_{max} in Fig. 42 when ϕ is 0.001. Comparison of Fig. 46 and Fig. 42 uncovers that the optimized design

with one daughter fin attached to each mother fins (Fig. 46 with ϕ=0.001) corresponds to the thermal resistance value of ϕ=0.002 in Fig. 42. This result is essential because it uncovers that the thermal resistance can be decreased with geometric optimization instead of high conductivity material volume twice.

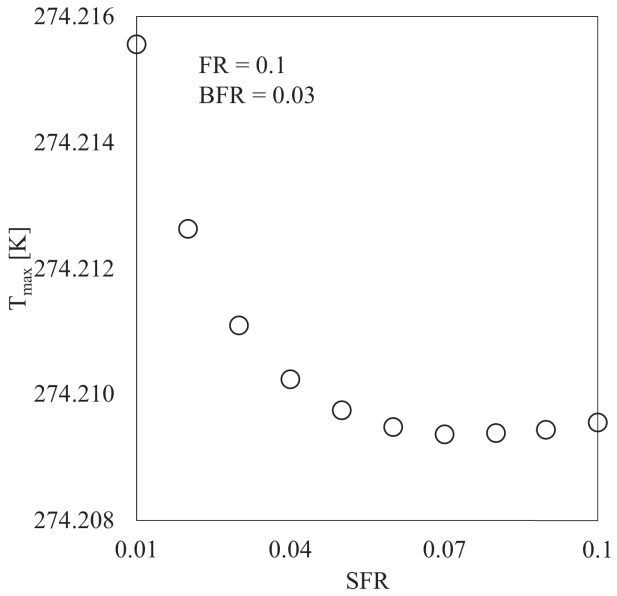

Figure 44. T_{max} relative to SFR for BFR=0.03 and FR=0.1

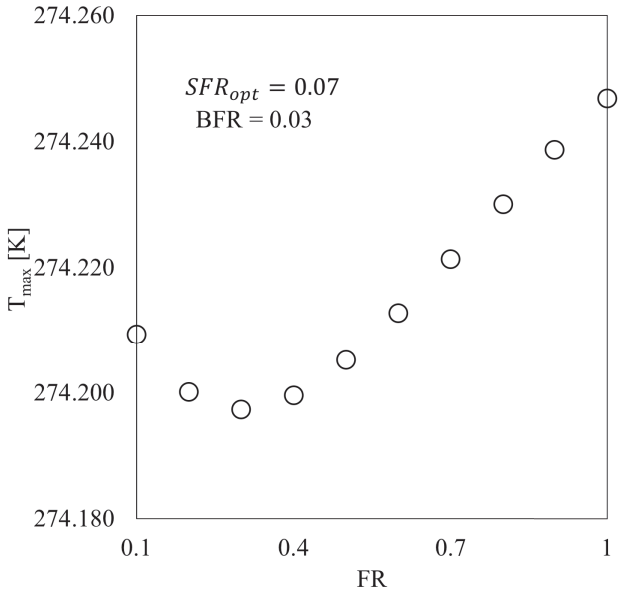

Figure 45. T_{max} relative to FR for BFR=0.03 and SFR_{opt}=0.07

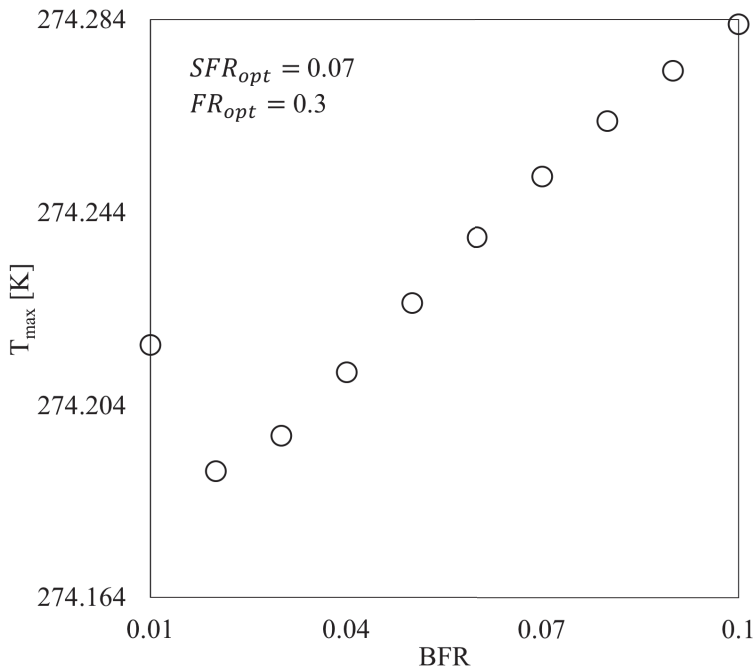

Figure 46. T_{max} relative to BFR for SFR_{opt}=0.07 and FR_{opt}=0.3

3.2.3. Two Daughter Fins Addition

Next, consider two daughter fins are attached to the tip of each mother fin. First, two daughter fins were attached to the tip of the mother fins. However, the thermal resistance did not decrease in this case. Then, the second fin was attached to the perimeter of the first daughter fin in order to see its effect. Here, one of the daughter fins was placed with an angle $(10°)$ at the tip of the mother fin which is shown in Figure 47. Furthermore, optimum location for the second daughter fin was surveyed along L_s. Figure 48 shows that there is a location where T_{max} is minimum, which is $0.7 \times L_s$. Thus, the second additional fins were placed at this point, and optimum values for SFR, FR and BFR were uncovered for this fin position. This result may look unexpected. However, as a snowflake growing the thickness of each branch increases, and the thickness is smaller at the tip. Fig. 48 shows this should be the case and if the thickness of the tip of the fin and daughter fin thickness are the same. Then, the position of bifurcation should also be located at a point where is $0.7 \times L_s$.

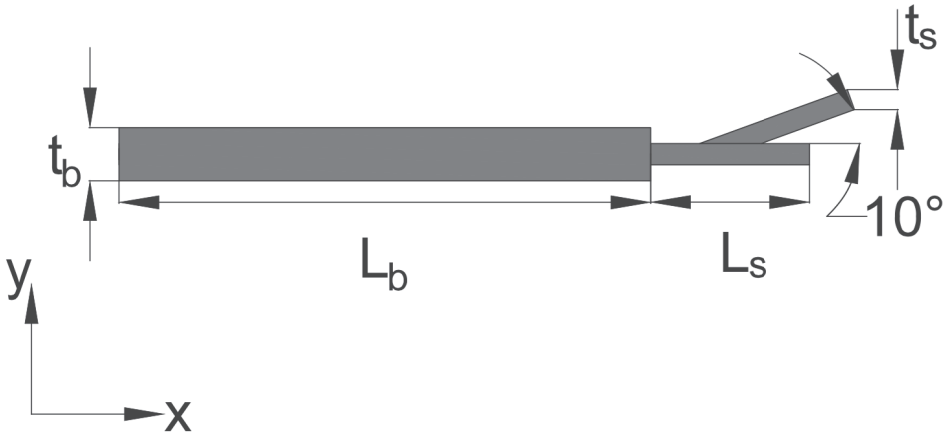

Figure 47. Placement of the second daughter (small) fin

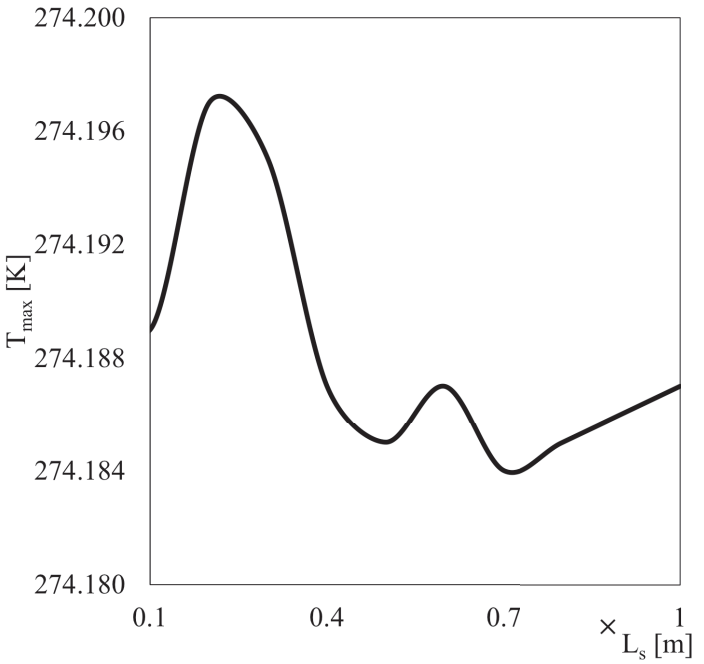

Figure 48. Optimum location results for the second daughter fins

Figures 49, 50 and 51 show the SFR_{opt}, FR_{opt} and BFR_{opt} corresponding to the minimum T_{max} exist, respectively. Here, the optimal length scales are SFR_{opt} = 0.07, FR_{opt} = 0.2 and BFR_{opt} = 0.02.

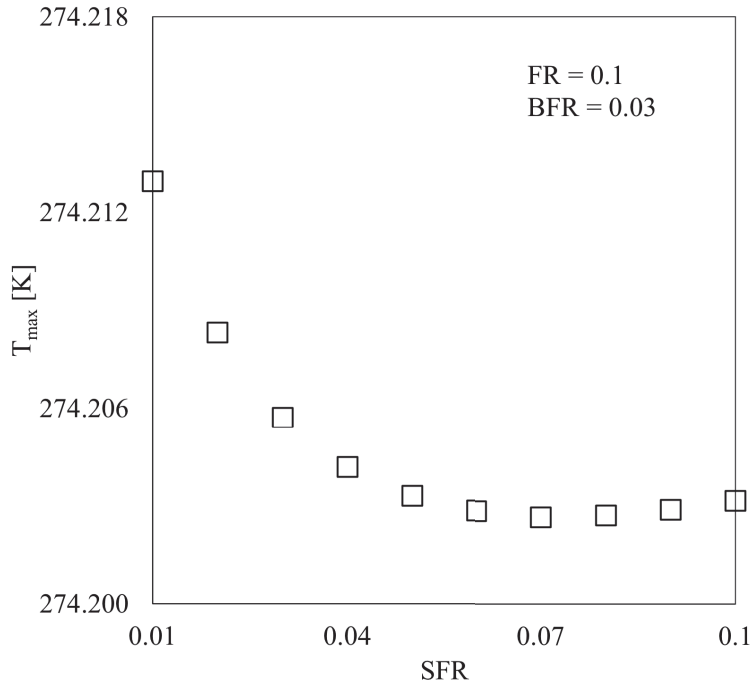

Figure 49. T_{max} relative to SFR for BFR=0.03 and FR=0.1

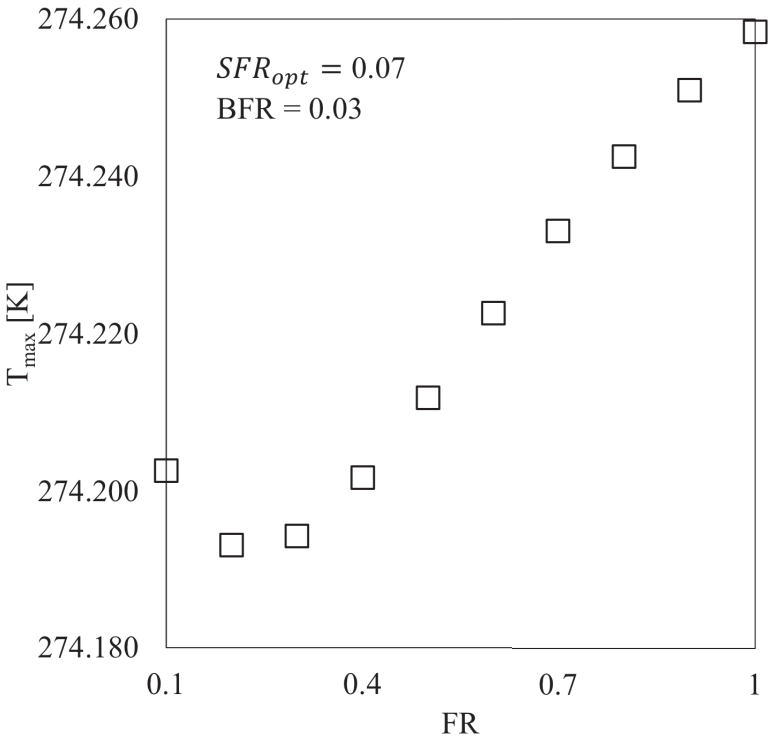

Figure 50. T_{max} relative to FR for BFR=0.03 and SFR_{opt}=0.07

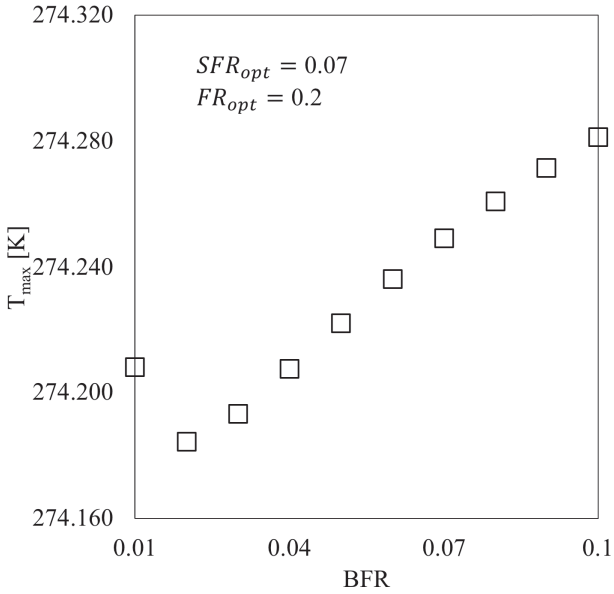

Figure 51. T_{max} relative to BFR for SFR_{opt}=0.07 and FR_{opt}=0.2

3.2.4. Three Daughter Fins Addition

Next, consider the addition of third small fins, which are symmetrical to the second daughter fins as shown Figure 52. The optimal length scales are uncovered in this section similar fashion to the two daughter fins addition section.

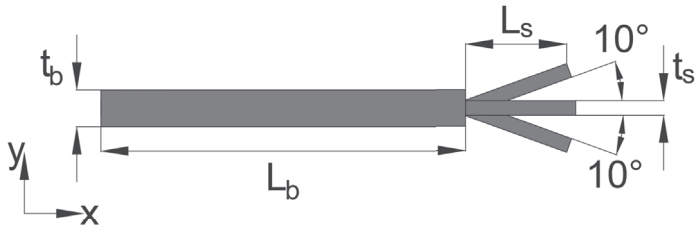

Figure 52. Placement of the third daughter fin

Figures 53, 54 and 55 indicate the optimum fin ratios for adding three daughter fins. SFR_{opt} is 0.02, and it is less than SFR_{opt} values in the previous two daughter fin additions, which are 0.07 for both of them. In addition, FR_{opt} is 0.3, like one daughter fin addition, and BFR_{opt} is 0.02, which is the same for all daughter fin additions.

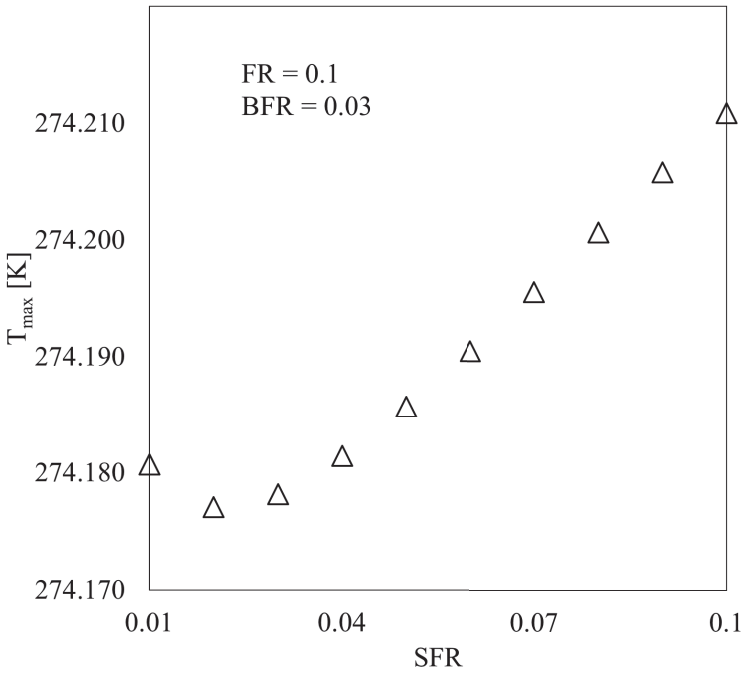

Figure 53. T_{max} relative to SFR for BFR=0.02 and FR=0.2

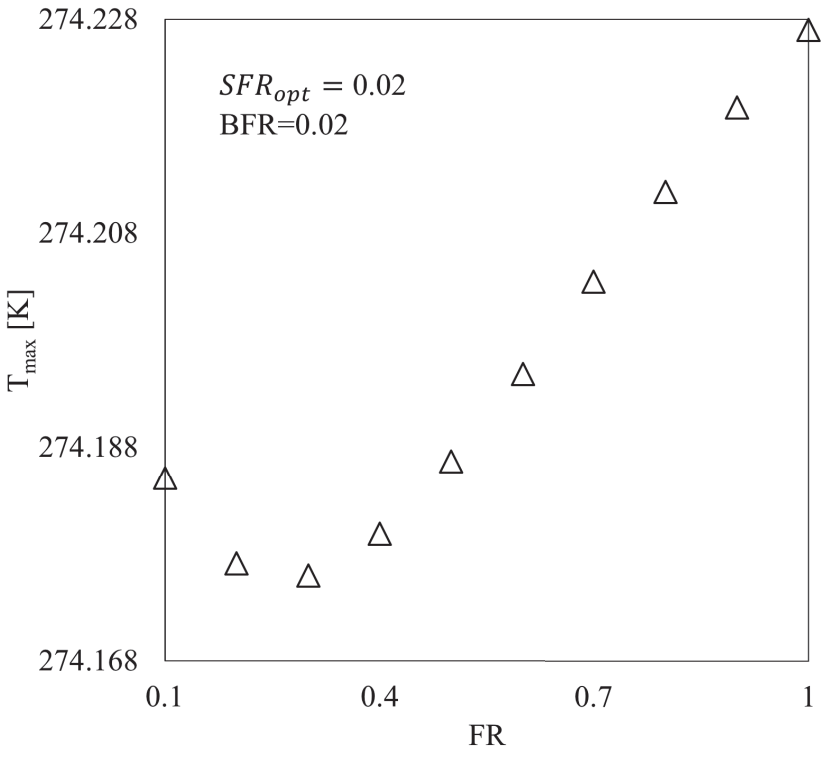

Figure 54. T_{max} relative to FR for BFR=0.02 and SFR_{opt}=0.02

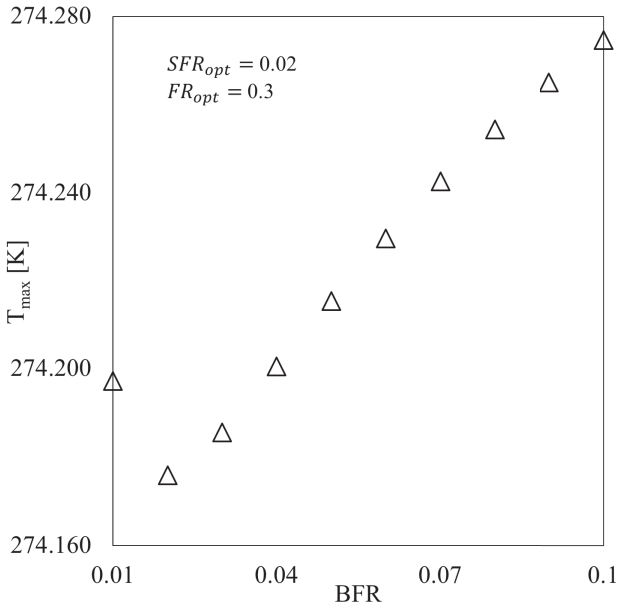

Figure 55. T_{max} relative to BFR for SFR_{opt}=0.02 and FR_{opt}=0.3

3.3. Optimum Angle for Daughter Fins

In the second assembly the daughter fins were placed with an angle ($\alpha = 10°$). Next, the effect of angle α on the thermal resistance should be uncovered. Therefore, α was varied in between 10° and 60° in order to uncover the design corresponding to the minimum thermal resistance. Figure 56 shows that the T_{max} decreases as the α increases from 10° to 15°. Then, T_{max} increases as α increases from 15° to 60°. Figure 56 indicates that minimum thermal resistance in achieved with $\alpha = 15°$ when the optimized fin ratios as given in Figures 53, 54 and 55.

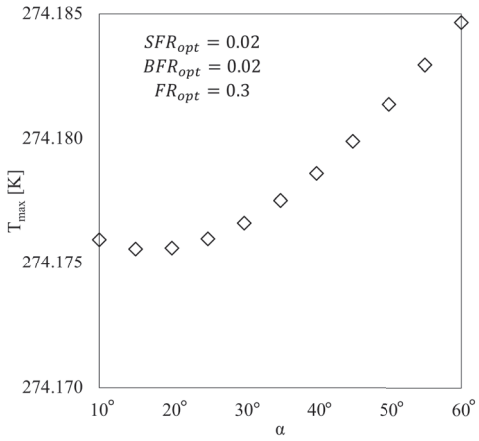

Figure 56. T_{max} relative to angle (α)

3.4. The Third Assembly

The results have uncovered that the daughter fins should be attached to the perimeter of the daughter fin in the position of $0.7 \times L_b$ with an α_{opt}. Next, we use this result to insert new level of daughter fins attached to the perimeter of the mother fins as shown in Figure 57. The thickness and the length of the new inserts should be bigger than the daughter fins discussed in previous section in order to decrease thermal resistance as mentioned by Bejan and Lorente [3]. Therefore, the length and thickness of the new addition is $2 \times L_s$ and $2 \times t_s$, respectively. Furthermore, the results of the second assembly also show that the position of the inserted fins to the perimeter affect the thermal resistance. Therefore, the location of the base of these new additions were varied along the length of the mother fin.

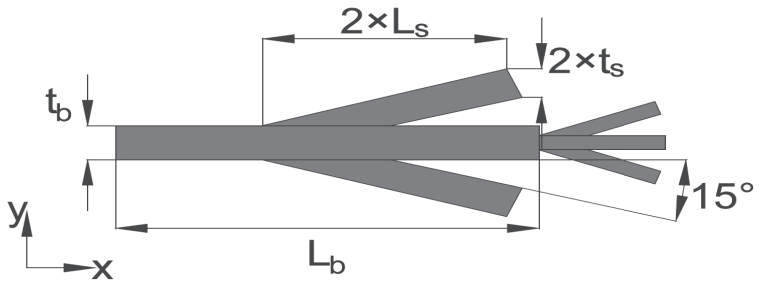

Figure 57. Placement of the daughter fins in the third assembly

Figures 58, 59 and 60 show that how the fin geometric ratios of SFR, FR and BFR affect the T_{max} when the position of the third assembly is $0.5 \times L_b$, $0.7 \times L_b$, and $0.8 \times L_b$. Figure 58 shows the effect of SFR ratio on the thermal resistance. T_{max} becomes the minimum with SFR = 0.02 for all location of the third assembly base. In addition, the thermal resistance is minimum when the base location of the third assembly is $0.8 \times L_b$. Figure 59 shows the effect of FR ratio on T_{max} for various locations of the third assembly of fins. T_{max} is minimum with FR = 0.4 when the position is $0.7 \times L_b$ and $0.8 \times L_b$. However, FR ratio corresponding to the minimum T_{max} is 0.6 with $0.5 \times L_b$ position. Figure 59 also shows that minimum T_{max} is achieved when the position is

$0.5 \times L_b$. Figure 60 shows the effect of BFR ratio on T_{max} with the SFR_{opt} and FR_{opt} in Figs. 58 and 59. T_{max} is minimum when position of the third assembly is $0.5 \times L_b$ and SFR = 0.02, FR = 0.6 and BFR = 0.03. Comparison of Figures 56 and 60 uncovers that the thermal resistance with optimized third assembly becomes smaller than the optimized second assembly design for the constant fin area. Therefore, the results uncover that the thicker fins should be attached to the perimeter of the mother fin and thinner fins should be attached to the perimeter of the mother fins to decrease the thermal resistance. Furthermore, the comparison of Figures 48 and 60 also indicate that the position of the attached fin to the perimeter should be shifted along the length of the mother fin to minimize thermal resistance, i.e. $0.5 \times L_b$ and $0.7 \times L_s$ are the positions for additional fins to be inserted in order to minimize thermal resistance. The reason for this position shift is related with the growth of the thermal boundary layers. In order to minimize the thermal resistance, the fins should be attached where the domain around the fin is not heated from previous section of assembly. Therefore, the position for the next assembly of the fins should be further from previous section of the fins.

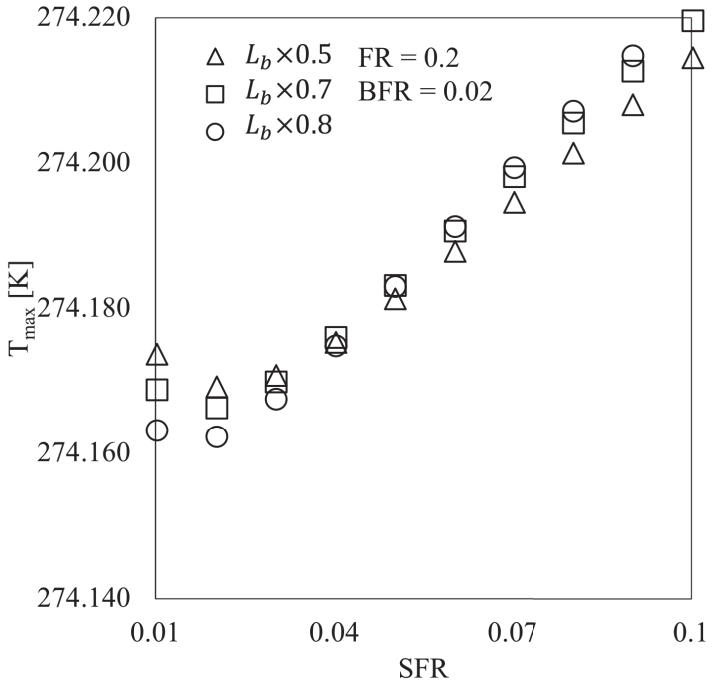

Figure 58. T_{max} relative to SFR for various locations of the third assembly when FR=0.2 and BFR=0.02

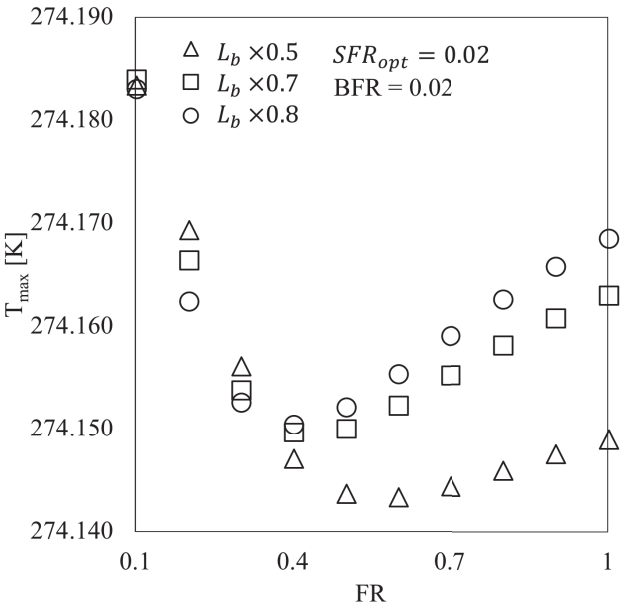

Figure 59. T_{max} relative to FR for various locations of the third assembly when SFR_{opt}=0.02 and BFR=0.02

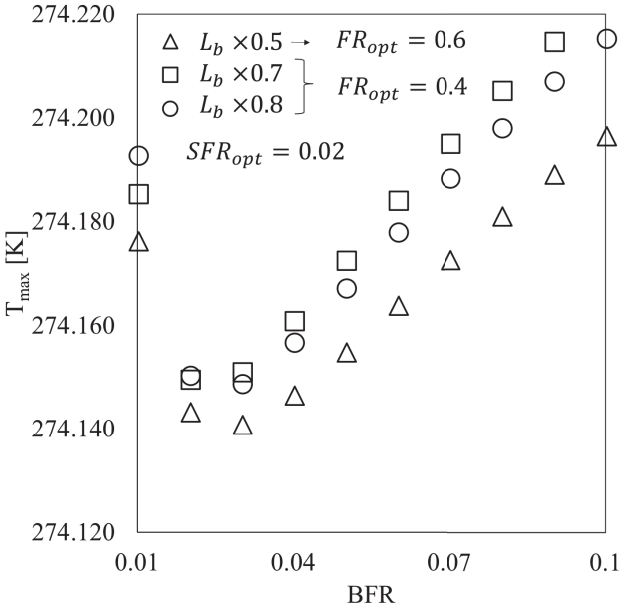

Figure 60. T_{max} relative to BFR for various locations of the third assembly when SFR_{opt}=0.02 and FR_{opt}=0.4 and 0.6

3.5. Optimized Snowflake Shape High-conductivity Pathways vs. Real Snowflake

After the third assembly, optimization results indicate that the optimization of the domain shown in Fig. 41 is a snowflake, as shown in Figure 61a. Optimized mother and

daughter fins were placed at their optimum locations. Optimized configuration includes 6 number of mother fins and they are identical. It is a characteristic feature of real snowflake shape because of different surface orientations as growing different rates [36]. However, there are 30 daughter fins, and they are not the same. The daughter fins at the perimeter of the mother fins are larger than the daughter fins at the perimeter of the daughter fins because the fins at the tips grow faster [36]. In addition, Figure 61b shows a specific snowflake shape. Comparison of optimized configuration the real snowflake as shown in Figs. 61a and b, it is obvious that the pathways near the center is thicker than the ones further and at the tip. Other common point between optimized configuration and real snowflake is the number of daughter fins. Our optimized configuration represents the minimum thermal resistance for a point heat source domain. Therefore, it is clear that snowflake represents the shape of minimum thermal resistance in the nature.

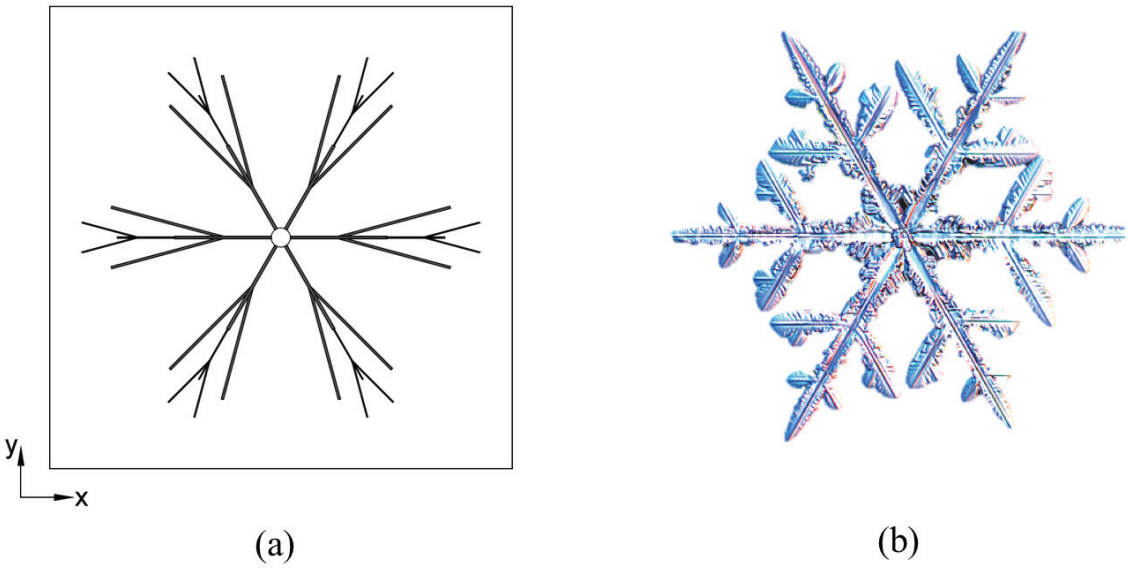

Figure 61. (a) The view of optimized geometry with a point heat source; (b) The real snowflake shape similar to optimized geometry [35]

3.6. The Effect of Heat Flux

In order to uncover the effect of heat flux on SFR_{opt}, FR_{opt} and BFR_{opt}, three distinct heat flux values were also studied such as 3, 5 and 10 $\mathrm{W/m^2}$. Figures 62, 63 and 64 show the effect of fin geometry ratios on T_{max} for various heat flux values supplied

from the perimeter of the heat source as shown in Figure 41. The results of Figs. 62, 63 and 64 show that the optimal ratios corresponding to the minimum thermal resistance becomes different than the previous cases, q''=1 $\mathrm{W/m^2}$, as the heat flux value increases. This is expected because there are many distinct shapes of snowflakes. The results confirm that each snowflake shape in the nature corresponds to the minimization of the thermal resistance and their shape is different due to the boundary conditions they had while they were being formed.

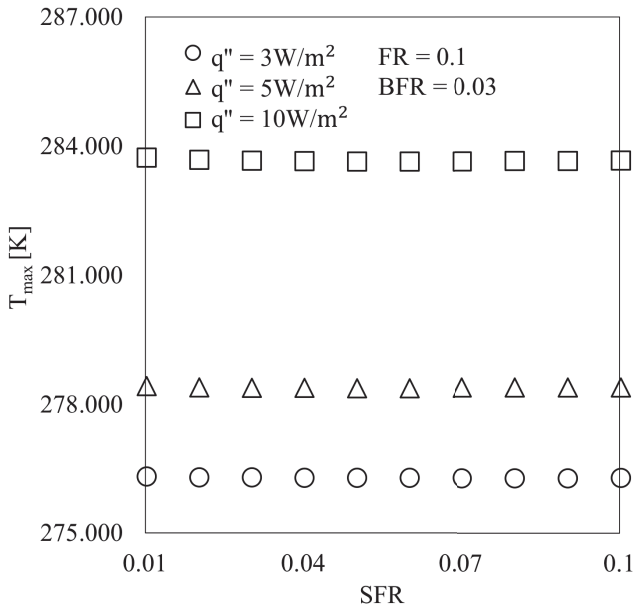

Figure 62. T_{max} relative to SFR for q''= 3, 5 and 10 W/m^2

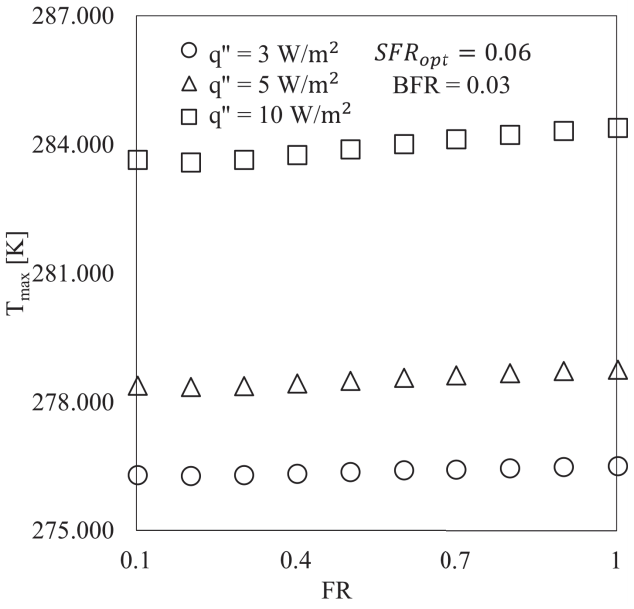

Figure 63. T_{max} relative to FR for q''= 3, 5 and 10 W/m^2

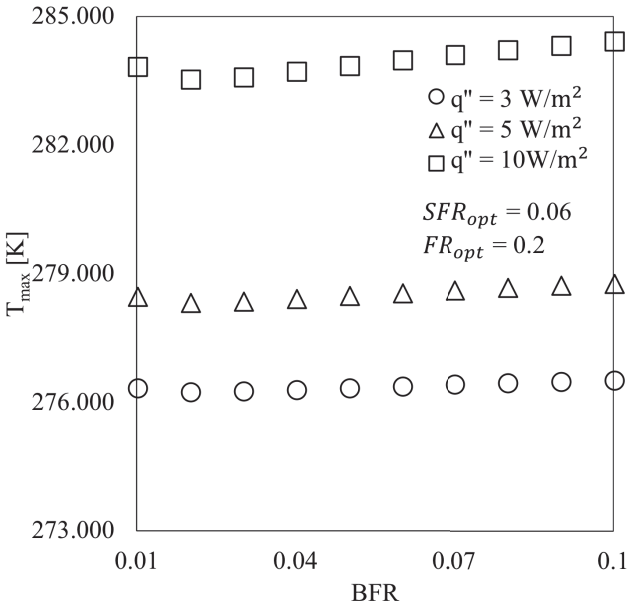

Figure 64. T_{max} relative to BFR for q''= 3, 5 and 10 W/m^2

3.7. The Effect of Thermal Conductivity

In this section the effect of thermal conductivity was analyzed. The ratio of thermal conductivities k was varied in order to uncover its effect on the optimized geometry. Figures 65, 66 and 67 document the geometric parameters corresponding to the minimum T_{max} such as, SFR_{opt}, FR_{opt} and BFR_{opt}. SFR_{opt} is 0.06 and FR_{opt} is 0.2 when *k* is varying from 50, 80 to 100. However, when *k* becomes 200 and more, SFR_{opt} decreases to 0.05 and 0.03, respectively. The order of FR_{opt} is approximately the same (0.2 and 0.3) when *k* varies. In addition, Figure 67 shows that BFR_{opt} values exist for *k* = 50, 80 and 100. However, there are no BFR_{opt} when *k* = 200 and greater.

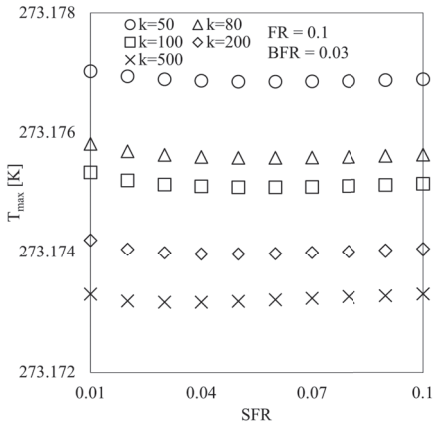

Figure 65. T_{max} relative to SFR for *k* = 50, 80, 100, 200 and 500

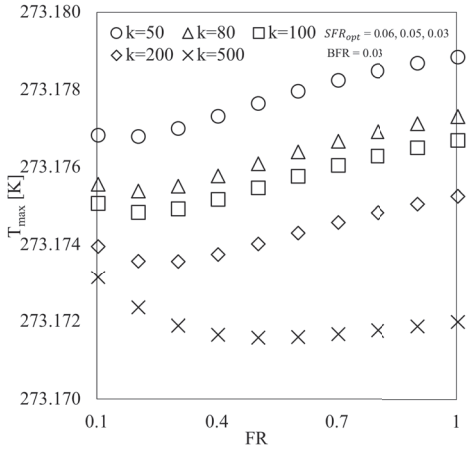

Figure 66. T_{max} relative to FR for k = 50, 80, 100, 200 and 500

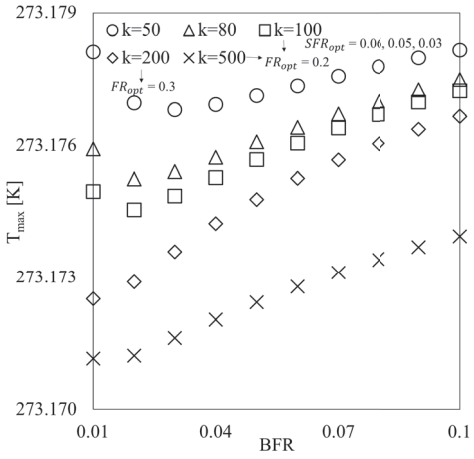

Figure 67. T_{max} relative to BFR for k = 50, 80, 100, 200 and 500

3.8. The Effect of Volume Fraction (ϕ)

In this part, the effect of ϕ was analyzed by using greater ϕ values in the previous three assemblies. The first assembly and three assembly steps in the second assembly were repeated for greater ϕ and q''. ϕ is varied between 0.01 and 0.05, and q'' is 100 W/m^2.

3.8.1. The first assembly for greater ϕ

Figure 68 indicates that the variation in T_{max} for 4, 6 and 8 number of fins while ϕ is varied. 6 number of fins corresponds to minimum T_{max} value for each ϕ value. This

result is coherent with the result in section 3.1. Comparison of Fig. 42 and Fig. 68 shows that when ϕ and q'' are increased, the decrease in T_{max} is obtained significantly.

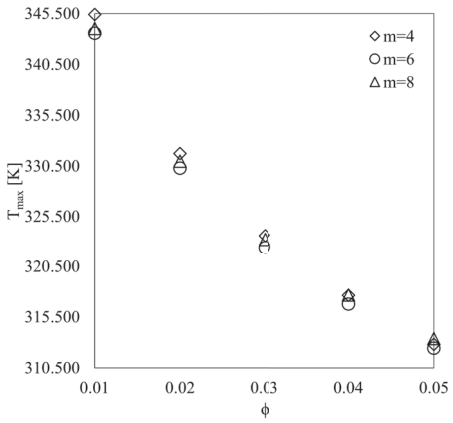

Figure 68. T_{max} relative to ϕ for various number of mother fins

3.8.2. The second assembly for greater ϕ

After the first assembly results as ϕ is between 0.01 and 0.05, the second assembly was analyzed when ϕ is 0.02 with three daughter fins addition separately. Figures 69, 70 and 71 shows the optimization results with one daughter fin addition in the second assembly. SFR_{opt} is 0.05 as shown in Fig.69. FR_{opt} is 0.3 as shown in Fig. 70, and BFR_{opt} is 0.02 as shown in Fig.71. These results show that minimum T_{max} decreases during optimization. Moreover, comparison of Figs. 68 and 71 indicates that T_{max} in Fig.71 is less than T_{max} in Fig. 68 for ϕ is 0.02.

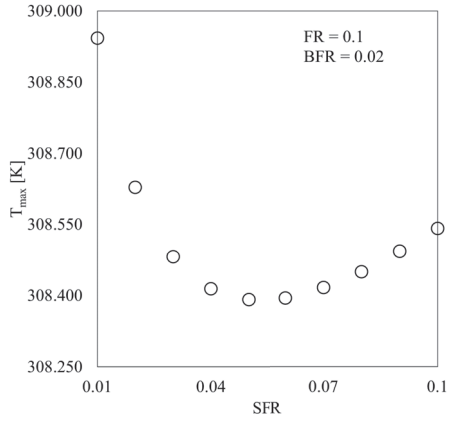

Figure 69. T_{max} relative to SFR for FR=0.1 and BFR=0.02

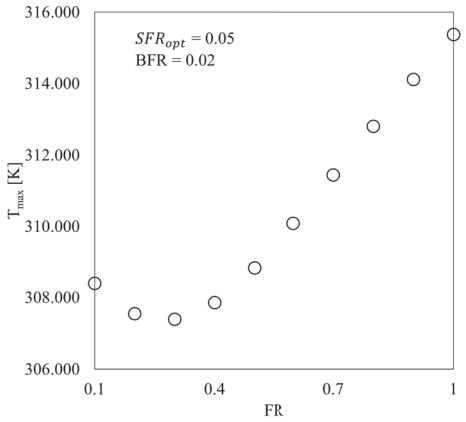

Figure 70. T_{max} relative to FR for SFR_{opt}=0.05 and BFR=0.02

After one daughter fin addition, two daughter fins were attached to the tip of the mother fins, like in section 3.2.3. Figs. 72, 73 and 74 indicates the optimization results. SFR_{opt} is 0.05, FR_{opt} is 0.3 and BFR_{opt} is 0.02 for greater ϕ and q''.

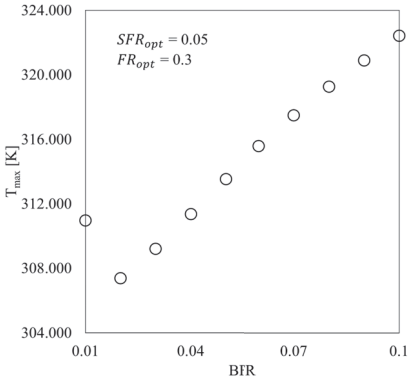

Figure 71. T_{max} relative to BFR for SFR_{opt}=0.05 and FR_{opt}=0.3

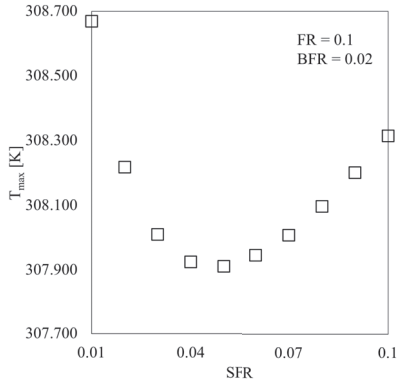

Figure 72. T_{max} relative to SFR for FR=0.1 and BFR=0.02

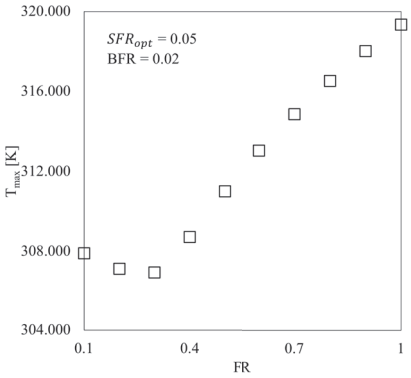

Figure 73. T_{max} relative to FR for SFR_{opt}=0.05 and BFR=0.02

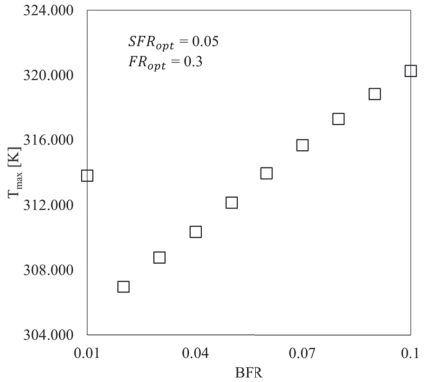

Figure 74. T_{max} relative to BFR for SFR_{opt}=0.05 and FR_{opt}=0.3

Next, three daughter fins were attached the tip of the mother fins as shown in Fig. 52. Optimization results are shown in Figures 75, 76 and 77. Here, SFR_{opt} is 0.02, FR_{opt} is 0.5 and BFR_{opt} is 0.02.

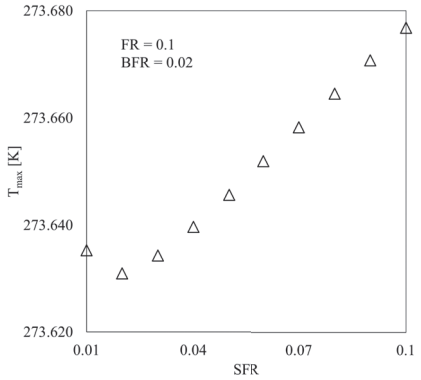

Figure 75. T_{max} relative to SFR for FR=0.1 and BFR=0.02

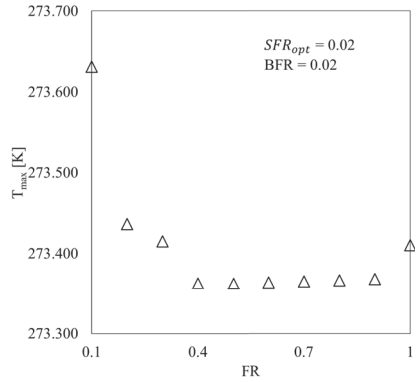

Figure 76. T_{max} relative to SFR for SFR_{opt}=0.02 and BFR=0.02

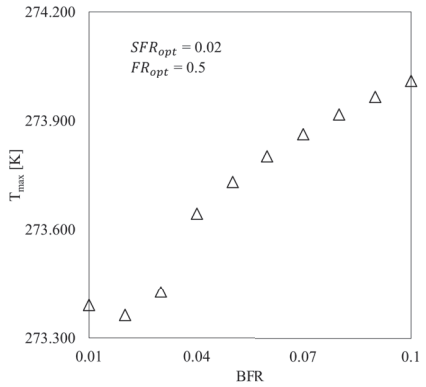

Figure 77. T_{max} relative to BFR for SFR_{opt}=0.02 and FR_{opt}=0.5

When the results in sections 3.1, 3.2 and 3.8 are compared, it is clear that the reduction in T_{max} (thermal resistance) is greater in section 3.8 than sections 3.1 and 3.2. In addition, optimum number of mother fins 6 for both 3.1 and 3.8.1. Furthermore, SFR_{opt} for one daughter fin and two daughter fins addition in 3.8.2 are less than in 3.2.2 and 3.2.3. However, SFR_{opt} is the same three daughter fins addition in 3.8.2 and 3.2.4. FR_{opt} is the same for one daughter fin addition in 3.8.2 and 3.2.2. In 3.8.2 for two daughter fins addition FR_{opt} is greater than FR_{opt} in 3.2.3. Similarly, FR_{opt} for three daughter fins addition in 3.8.2 is greater than FR_{opt} in 3.2.4. On the other hand, BFR_{opt} is the same for all daughter fin addition steps in 3.8.2 and in 3.2.

CHAPTER 4

CONCLUSION

This study shows that thermal resistance reduction in a domain in which a point heat source exists at the center. High-conductivity material (rectangular fins) were placed at the perimeter of the heat source in order to minimize excess maximum temperature (T_{max}). The geometry of high conductive pathways was designed according to Constructal Theory. The geometry of mother fins was uncovered in the first assembly. For optimum mother geometry, $\phi = (A_f/A_s)$ was varied from 0.001 to 0.01 where fin ratio ($t_f/L_f = 0.1$) was constant. Figure 42 indicates the T_{max} relation with area fraction when number of fins vary, and it uncovers the two extrema. The first extremum is that T_{max} exists when the number of fins is low because of large spacing between the fins. The second extremum is that short spacing between fins results in overlapping thermal boundary layer, so heat transfer rate decreases. As shown in Figure 42, when $\phi < 0.004$, minimum T_{max} exists for 8 number of fins, but when $\phi > 0.004$, minimum T_{max} exists for 6 number of fins. In this condition, 6 number of fins was accepted as the optimum number of mother fins because when $\phi < 0.004$, the temperature difference between them is not high, and while ϕ increases, minimum T_{max} exists for 6 number of fins. After deciding optimum number of mother fins, geometry optimization was continued with addition of daughter fins because Bejan and Lorente [3] showed that additional branches can be used in order to decrease thermal resistance. Therefore, in the second assembly, daughter fins were attached to the tip of mother fins. Three distinct fin ratios, SFR (t_s/L_s), FR (L_s/L_b) and BFR (t_b/L_b), were defined in order to obtain optimum length scales of the fins and the number of daughter fins. There are 3 steps for daughter fins addition. In each step one daughter fin was added, and optimum fin ratios were documented. Table 3 shows the optimum fin ratio values and minimum T_{max} relative to the number of daughter fins. When the number of daughter fins is increased, SFR_{opt} decreases, which means daughter fins become thinner. In addition, the number of daughter fins does not affect FR_{opt}, so optimum ratio between daughter and mother fins is constant. Similarly, BFR_{opt} is independent from the number of daughter fins. In

addition, optimum daughter fin location was uncovered, which is at $0.7 \times L_s$ as shown in Figure 48. Optimum angle α is 15° for minimum T_{max} as shown in Figure 56.

Table 3. Optimum fin ratio values and minimum T_{max} values with respect to the number of daughter fins

# of daughter fins	SFR_{opt}	FR_{opt}	BFR_{opt}	min.T_{max} [K]
1	0.07	0.3	0.02	274.190
2	0.07	0.2	0.02	274.184
3	0.02	0.5	0.02	274.176

After the second assembly, third assembly uncovers that the thermal resistance can be decreased even more addition of thicker daughter fins to the periphery of the mother fins. The results indicate that daughter fins tend to form along L_b where temperature is higher in Figure 60, and these daughter fins are longer and thicker than the daughter fins attached to tip of mother fins in the second assembly. Third assembly provides significant reduction in T_{max}, Fig. 60. Table 4 shows the optimum geometric length scale ratios for the third assembly relative to the position of the daughter fins along the surface of the mother fin.

Table 4. The third assembly optimization results

daughter fins placement	SFR_{opt}	FR_{opt}	BFR_{opt}
$L_b \times 0.5$	0.02	0.6	0.03
$L_b \times 0.7$	0.02	0.4	0.02
$L_b \times 0.8$	0.02	0.4	0.03

Then, how the heat flux affects the optimum fin ratios were uncovered by varying the heat flux rate. The results show that the design corresponding to the minimum T_{max} (minimum thermal resistance) varies as the heat flux varies. This condition is coherent with snowflake formation because each snowflake shape is unique (subjected to different boundary conditions). In addition, the effect of thermal conductivity on the geometry optimization was analyzed by using various thermal conductivity (k) values. The results show that k has an effect on optimum fin ratios, which are shown in Table 5. It shows that

when the k is in between 50 and 100, there is no change for fin ratios, except BFR_{opt} for k = 50. However, when the k is equal to greater than 100, SFR_{opt} begins to decrease. However, FR_{opt} is approximately the same, and it is 0.2.

Table 5. The effect of the thermal conductivity on optimum fin ratios

k	SFR_{opt}	FR_{opt}	BFR_{opt}
50	0.06	0.2	0.03
80	0.06	0.2	0.02
100	0.06	0.2	0.02
200	0.05	0.3	0.01
500	0.03	0.2	0.01

Lastly, the effect of volume fraction (ϕ) was analyzed. The results show that increase in volume fraction provides higher decrease in minimum T_{max} in the first and second assembly. It affects the optimum fin ratio values as shown in Table 6.

Table 6. The optimization results of the second assembly with greater ϕ and q''

# of daughter fins	SFR_{opt}	FR_{opt}	BFR_{opt}	min.T_{max} [K]
1	0.05	0.3	0.02	307.5
2	0.05	0.3	0.02	306.9
3	0.02	0.5	0.02	273.3

The optimum configuration corresponding to the minimum T_{max} for the given boundary conditions and for point to volume domain is snowflake shaped. In this study we reduced the thermal resistance by embedded high conductivity material (rectangular fin) for a domain in which includes a point heat source. Here, the snowflake design was not dictated but uncovered as the design with minimum thermal resistance. It is an expected result since snowflake structure forms in order to decrease the free energy for fixed boundary conditions [36]. In addition, this result show that snowflake designs are good distributors and collectors for point to volume flows. This also explains their usage in engineering applications from the observations of scientists. The results of the current

study also in agreement with Constructal Theory and the current literature for the design to be altered in order to provide the smallest resistance to the flow as the conditions vary.

REFERENCES

1. S. Kakaç, H. Yüncü and K. Hijikata. (1994). *Cooling of Electronic Systems.* Dordrecht: Kluwer Academic Publishers.

2. A. Bejan. (1997). Constructal theory network of conducting paths for cooling a heat generating volume. *International Journal of Heat and Mass Transfer, 40*, 799-816.

3. A. Bejan and S. Lorente. (2008). *Design with Constructal Theory.* New Jersey: John Wiley & Sons, Inc.

4. A. Bejan, V. Badescu and A. De Vos. (2000). Constructal theory of economics structure generation in space and time. *Energy Conversion and Management, 41*, 1429-1451.

5. A.H. Reis, A.F. Miguel and M. Aydın. (2004). Constructal theory of flow architecture of the lungs. *Medical Physics, 31*, 1135-1140.

6. A. Bejan and S. Lorente. (2006). Constructal theory of generation of configuration in nature and engineering. *Journal of Applied Physics, 100*.

7. A.V. Azad and M. Amidpour. (2011). Economic optimization of shell and tube heat exchanger based on constructal theory. *Energy, 36*, 1087-1096.

8. G.A. Ledezma, A. Bejan and M. Errera. (1997). Constructal tree networks for heat transfer. *Journal of Applied Physics, 82*, 89-100.

9. A. Bejan and M. Almogbel. (1999). Conduction trees with spacing at the tips. *International Journal of Heat and Mass Transfer, 42*, 3739-3756.

10. G. Lorenzini, C. Biserni and L.A.O. Rocha. (2013). Constructal design of non-uniform X-shaped conductive pathways for cooling. *International Journal of Thermal Sciences, 71*, 140-147.

11. M.R. Hajmohammadi, V.A. Abianeh, M. Moezzinajafabadi and M. Daneshi. (2013). Fork-shaped highly conductive pathways for maximum cooling in a heat generating piece. *Applied Thermal Engineering, 61*, 228-235.

12. M.R. Hajmohammadi, O.J. Shariatzadeh, M. Moulod and S.S. Nourazar. (2014). Phi and Psi shaped conductive routes for improved cooling in a heat generating piece. *International Journal of Thermal Sciences, 77*, 66-74.

13. C.D.S. Horbach, E.D. dos Santos, L.A. Isoldi and L.A.O. Rocha. (2014). Constructal design of Y-shaped conductive pathways for cooling a heat generating body. *Defect and Diffusion Forum. 358*, s. 245-260. Switzerland: Trans Tech Publications.

14. M.R. Hajmohammadi, G. Lorenzini, O.J. Shariatzadeh and C. Biserni. (2015). Evaluation in the design of V-shaped highly conductive pathways embedded in a heat-generating place. *Journal of Heat Transfer, 137*.

15. H. Feng, L. Chen, Z. Xie and F. Sun. (2015). Constructal design for "+" shaped high conductivity pathways over a square body. *International Journal of Heat and Mass Transfer, 91*, 162-169.

16. E. Cetkin and A. Oliani. (2015). The natural emergence of asymmetric tree-shaped pathways for cooling of a non-uniformly heated domain. *Journal of Applied Physics, 118*.

17. M. Eslami. (2016). Optimal conductive constructal configurations with "parallel design". *Energy Conversion and Management, 111*, 352-357.

18. G. Lorenzini, E.X. Barreto, C.C. Beckel, P.S. Schneider, L.A. Isoldi, E.D. dos Santos and L.A.O. Rocha. (2016). Constructal design of I-shaped high conductive pathway for cooling a heat-generating medium considering the thermal contact resistance. *International Journal of Heat and Mass Transfer, 93*, 770-777.

19. G. Lorenzini, E.X. Barreto, C.C. Beckel, P.S. Schneider, L.A. Isoldi, E.D. dos Santos and L.A.O. Rocha. (2017). Geometrical evaluation of T-shaped high conductive pathway with thermal contact resistance for cooling of heat-generating medium. *International Journal of Heat and Mass Transfer, 2017*, 1884-1893.

20. J. You, H. Feng, L. Chen and Z. Xie. (2018). Heat conduction constructal optimization for nonuniform heat generating area based on triangular element. *International Journal of Heat and Mass Transfer, 117*, 896-902.

21. C. Biserni, L.A.O. Rocha and A. Bejan. (2004). Inverted fins: geometric optimization of the intrusion into a conducting wall. *International Journal of Heat and Mass Transfer, 47*, 2577-2586.

22. G. Lorenzini and L.A.O Rocha. (2006). Constructal design of Y-shaped assembly of fins. *International Journal of Heat and Mass Transfer, 49*, 4552-4557.

23. G. Lorenzini and S. Moretti. (2007). Numerical analysis on heat removal form Y-shaped fins: efficiency and volume occupied for a new approach to performance optimisation. *International Journal of Thermal Sciences, 46*, 573-579.

24. Z. Xie, L. Chen and F. Sun. (2010). Constructal optimization of twice Y-shaped assemblies of fins by taking maximum thermal resistance minimization as objective. *Science China Technological Sciences, 53*, 2756-2764.

25. G. Lorenzini, C. Biserni, R.L. Correa, E.D. dos Santos, L.A. Isoldi and L.A.O. Rocha. (2014). Constructal design of T-shaped assemblies of fins cooling a cylindrical solid body. *International Journal of Thermal Sciences, 83*, 96-103.

26. E. Cetkin. (2015). Inverted fins for cooling of a non-unifomly heated domain. *Journal of Thermal Enginneering, 1*, 1-9.

27. H. Feng, L. Chen, Z. Xie and F. Sun. (2017). Constructal design for helm-shaped fin with internal heat sources. *Internal Journal of Heat and Mass Transfer, 110*, 1-6.

28. D. Conners. (2018, January 3). *How snowflakes get their shape*. Retrieved May 2018, from EarthSky: http://earthsky.org/earth/how-do-snowflakes-get-their-shape

29. K. Kikuchi, T. Kameda, K. Higuchi and A. Yamashita. (2013). A global classification of snow crystals, ice crystals and solid precipitation based on observations from middle latitudes to polar regions. *Atmospheric Research*(132-133), 460-472.

30. J. Tyynela, J. Leinonen, D. Moisseev and T. Nousiainen. (2011). Radar Backscattering from Snowflakes: comparison of fractal, aggregate and soft spheroid models. *Journal of Atmospheric and Oceanic Technology, 28*, 1365-1372.

31. H. Nowell, G. Liu and R. Honeyager. (2013). Modeling the microwave single-scattering properties of aggregate snowflakes. *Journal of Geophysical Research: Atmospheres, 118*, 7873-7885.

32. R. Albanese, R. Ambrosino and M. Mattei. (2014). A procedure for the design of snowflake magnetic configurations in tokamaks . *Plasma Physics and Controlled Fusion, 56*.

33. D.K. Lee, C.W. Ahn and H.J. Jeon. (2016). Web of carbon fibers coated with 3D snowflake-shaped Ni3S2/Ni produced by electroless Ni plating: a binder-free cathode electrode for lithium batteries. *Microelectonic Engineering, 166*, 1-4.

34. COMSOL Multiphysics 5.0, COMSOL Inc, 2014.

35. K.G. Libbrecht. (1999, February 1). *Snow Crystals*. Retrieved May 2018, from Snow Crystals.com: http://snowcrystals.com/

36. J.P. Sethna. (2006). *Statistical Mechanics Entropy, Order Parameters, and Complexity.* Ithaca, NY: Clarendon Press.